Current Topics in Electrochemistry
Vol. 17, 2012

Review

Recent progress in the electrochemistry of planar and reticulated vitreous carbon: Fundamentals and applications

M. I. Awad[1,2,*], M. M. Saleh[1,2,#] and T. Ohsaka[1,$]

[1]Department of Electronic Chemistry, Interdisciplinary Graduate School of Science and Engineering, Tokyo Institute of Technology, 4259 Nagatsuta, Midori-ku, Yokohama 226-8502, Japan.
[2]Chemistry Department, Faculty of Science, Cairo University, Cairo, Egypt

ABSTRACT

This review outlines the recent published works on the fundamental studies and electrochemical applications of glassy carbon in both forms, i.e., planar glassy carbon (GC) and reticulated vitreous carbon (RVC) electrodes. Special attention is placed on our recent works for using glassy carbon electrode in hydrogen evolution reaction (HER), oxygen reduction reaction (ORR) and oxygen evolution reaction (OER), and the relevant literature on these are also reviewed. This includes the use of electrochemically pretreated GC and modified GC electrodes. The effects of surface modification via oxidation of the GC were outlined.

KEYWORDS: reticulated vitreous carbon, glassy carbon, oxygen evolution, oxygen reduction, ozone electrogeneration

1. INTRODUCTION

Glassy carbon electrodes (GCEs) represent a main class of important electrode materials from both fundamental and application points of view. Many papers, review articles and several chapters in several books have been published in this area [1-5]. Glassy carbons have two forms; planar glassy carbon (GC) and reticulated vitreous carbon (RVC) electrodes. Advantages of carbon electrodes include wide potential window, low cost, relatively inert electrochemistry, and electrocatalytic activity for a variety of redox reactions. Both of them have common characteristics albeit RVC has more advantages from practical point of view since it has high surface to volume ratio which reduces the volume of the reactor of interest. Planar GC electrode, on the other hand, acquires its importance as an electrode for intensive fundamental studies in designing chemical and biochemical sensors and testing of electrocatalytic properties. In most of these applications GC with its ordinary properties cannot be used without modification. Surface of GC has high potential for chemical and electrochemical modifications, loading of precious metals and grafting [6-10]. One of the most important characteristics is the oxidation and reduction of organic and biological molecules in both aqueous and non-aqueous media [11-14]. Important applications also include batteries, supercapacitors and metals electrowining, and applications required ideal substrate for loading many catalysts [15-20].

The present review focuses on the properties of the GCE, its modification by electrochemical oxidation and its applications in hydrogen evolution reaction (HER), production of hydrogen peroxide (H_2O_2) and oxygen evolution reaction (OER).

2. Manufacture and properties of GC materials

Glassy carbon (GC) is made by heating different types of polymers. Polyacrylo-nitrile is a common

*mawad70@yahoo.co
#mahmoudsaleh90@yahoo.com
$ohsaka@echem.titech.ac.jp

candidate for this purpose. On heating the polymer under pressure in an inert atmosphere to 1000-3000°C, the heteroatoms are evaporated and only carbon remains [21, 22]. The C-C bonds in the polymer backbone do not break at these temperatures, so the carbon can form graphitic planes of only limited size [21]. The interplanar spacing is larger than that of highly ordered pyrolytic graphite (HOPG), about 3.6 Å, and the graphite structure cannot fully develop due to the unbroken C-C bonds. A general acceptable structure of GC is a randomly intertwined ribbon of graphitic planes, although the randomness results in significant uncertainty about the detailed microstructure [23, 24]. It is known that GC is about 60% as dense as HOPG and must contain many voids, but its disordered nature makes structural characterization difficult at the atomic level. GC may also be made from a reactive polymeric precursor at relatively low temperature (~700°C), which permits "doping" with various heteroatoms in the polymer, as well as the final product, including halogens, silicon, and metal catalysts [25, 26].

Reticulated vitreous carbon (RVC) is different than planar GC with its porous foam-like structure. The structure of RVC is achieved by polymerization of a resin combined with foaming agents, followed by carbonization [5]. A low volume disordered glassy porous carbon was obtained with some crystallographic order and a continuous skeletal structure. Classically, polyurethane and phenolic resins are used although furfuryl and epoxy resins can also be used; these have 3% and 50% 'carbon yield', respectively. The foam resin is, typically, dried and cured at 120°C then carbonised at 700-1100°C. The starting polymer and the temperature of the carbonization have a great influence on the physicochemical properties of glassy carbons [5]. Controlling parameters of the process include the solution viscosity, the concentration of resin, the type of solvent, the concentration of curing agents, the precursor foam pore size and the firing temperature. Glassy porous carbon can also be obtained from high molar mass thermoplastic carbons (pitch) [5, 27]. During the production of RVC, a linear shrinkage of approximately 30% occurs. The porosity (void fraction) of RVC range is between 0.90 and 0.97 depending on the ppi grade, and briefly speaking, a surface area of ≈65 cm^2 cm^{-3}, for the 100 ppi grade is obtained [28]. The honeycomb structure of the RVC is given in Fig. 1 A, B at different magnifications. The structure is formed by strands of carbon, also called struts that form a so-called trigonal strut, which appears like a triangle from above but is in fact more like a tetrahedron, with one of the strands hidden out of view under the others. Replication of this arrangement gives rigid structure to the RVC [5]. RVC does not combust after heating (less than 350°C) to bright incandescence in air followed by removal of the heat source. It is highly resistant to

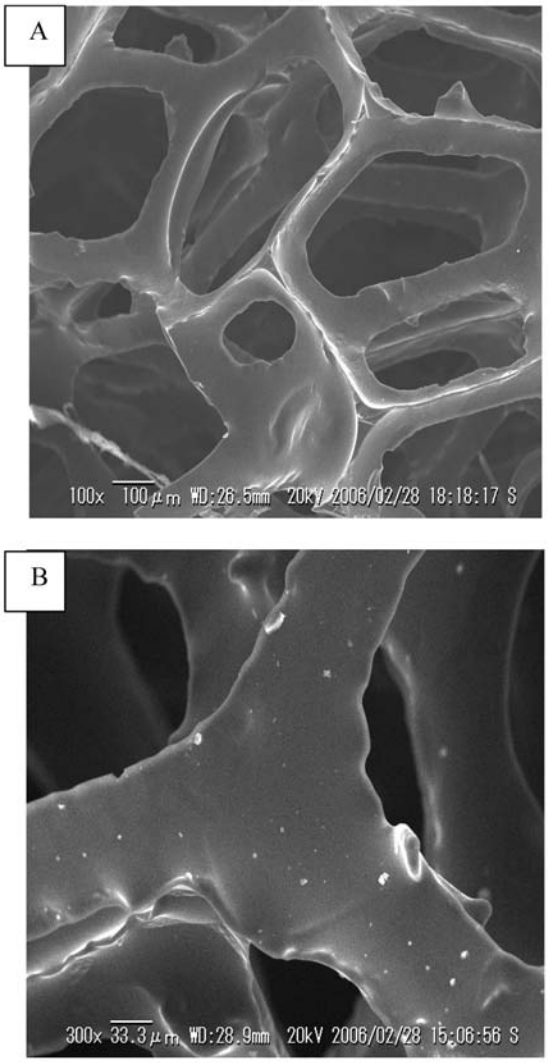

Fig. 1. SEM micrographs of RVC.

intercalation by materials that disintegrate graphite. GC in general is quite inert to different types of very reactive acids, bases, and organic solvents.

3. Modifications of GC surface

Modifications of GC electrodes include chemical and electrochemical oxidation, loading with precious metals (e.g, Ni, Pb Pt and Au) or grafting by loading organic molecules of specific fictionalization [29-40]. In this part we will focus on the electrochemical treatment by anodic oxidation of the GC electrodes. While the literature for the characterization and applications of chemically and electrochemically oxidized planar GC electrode are vast, only few papers have been reported in regard to the chemical or electrochemical oxidation of reticulated vitreous carbon (RVC) [41]. The electrochemical pretreatment procedures of planar GC electrode can be anodic oxidation [42-44] or cathodic reduction [44, 45]. The anodic activation may be in some cases followed by reduction or potential cycling [46-49]. The electrocatalytic activity of the pretreated GC depends not only on the pretreatment procedure but also on the electrochemical active species participating in the electrochemical reaction [32]. In other words, the pretreatment process may activate a specific electrochemical reaction. The oxidation has always been aimed to be applied in electroanalysis of biochemical species [50-52], electrochemical capacitors [15, 16] and important electrocatalytic reactions such as oxygen reduction reaction (ORR). Carbon electrodes have long been known for its selectivity for oxygen reduction to H_2O_2 [53]. It has been reported in literature that anodically oxidized glassy carbon electrode imparts better electrocatalytic activity and stability behavior towards oxygen reduction both in acid and alkaline solutions [29, 54, 55].

3.1. Characterization of electrochemically oxidized GC

The oxidation of three types of electrodes was conducted in order to compare their behaviors during the course of the oxidation in acid solution. These are planar GC and RVC electrodes (as flooded (stationary solution) and flow-through porous electrodes). The flow system and the arrangement of the flow-through porous electrode is given in Fig. 2. Oxidation of the three electrodes

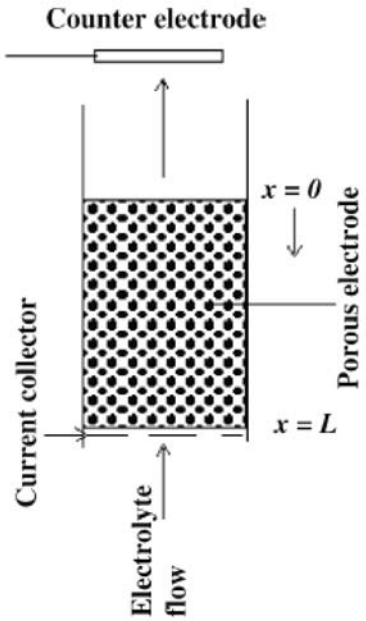

Fig. 2. Schematic of the cell arrangement and flow direction.

in 0.1 M H_2SO_4 was performed potentiostatically at potential of 2 V (SCE). Figures 3A-C show current transient of the oxidation process of the three electrodes for specific time periods. For the flow-through porous electrode the flow rate was 0.08 cm s^{-1}. The *i-t* relations are similar for all the electrodes. The only difference is the maximum shown for the planar GC electrode after about 30 s. The curves for the planar GC electrode are similar to that obtained in literature for GC [33]. The obtained high current at the beginning was attributed to the charging of the double layer. The current decreases to a minimum value at about ten seconds and begins to increase again to reach a constant value. The current increase in Fig. 3 corresponds to the activation of the electrode process towards water oxidation [33]. The increase in current reaches its saturation limit once the water oxidation process is catalyzed to its possible maximum extent. The assignment of the increase in the current reaching its saturation value to electrolytic oxidation of water was previously proved by in situ measuring of the dissolved oxygen concentration where the oxygen concentration was found to increase immediately after applying the anodization potential [33]. Note that the initial high currents in curves b are larger

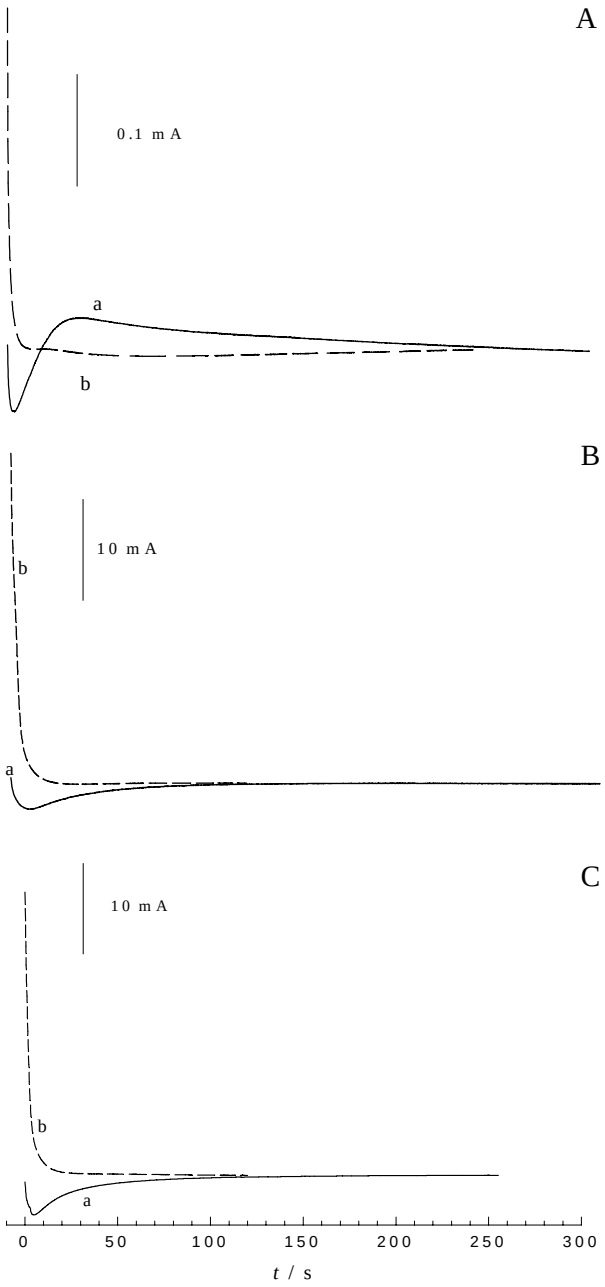

Fig. 3. Current-time relations for the anodic oxidation of different electrodes obtained by applying constant potential of 2.0 V for 5 min.; A) GC, B) flooded RVC and C) flow-through porous RVC electrode (in 0.1 M H_2SO_4 flowing at 0.08 cm s^{-1}).

than the initial currents of the fresh electrodes due to increase of the surface area and hence increase of the charging current. It can be concluded that the electrolyte flow does not affect the general features of the i-t curve as evident from Fig. 3B and C.

Shown in Figure 4 are SEM images of different sections (slices) of RVC flow-through porous electrode obtained after oxidation for 20 min at 2 V. The electrolyte was 0.1 M H_2SO_4 flowing at 0.08 cm s^{-1}. We used the 20 min oxidation here in order to obtain a considerable penetration depth of the current to the interior of the porous electrode. The roughness is taken as a measure of the oxidation extent [6]. As shown from the figure the roughness decreases as going down from the front of the electrode at $x = 0$ to the back at $x = 2$ cm for an electrode with 3 cm thickness. The image at 2 cm is completely smooth indicating lower extent of oxidation. The images reveal that only about one half of the porous electrode was subjected to stronger oxidation. The non-uniform distributions of the oxidation extent are attributed to the non-uniform distributions of the potential and current within the bed [56, 57]. At the present case the mixed ohmic and kinetic charge transfer resistances may affect the present current distributions within the porous electrode. In principle, optimum conditions e.g., higher electrolyte conductivity and thinner electrodes could be chosen to obtain a more uniform distribution of the oxidation extent within the RVC matrix.

X-ray photoelectron spectroscopy (XPS) is a strong surface analytical technique. It is widely used for probing the surface oxygen concentration and the surface functional groups on carbon electrodes [58, 59]. It has been utilized as an efficient tool for the characterization of carbon electrode pretreatment. A wide range of survey spectrum of plain (untreated) RVC sample was taken (data are not shown) and as expected the spectrum shows only two peaks at binding energies of 284.1 and 532.0 eV corresponding to carbon and oxygen, respectively, in agreement with the literature [60]. Only short range spectra for oxygen and carbon are shown in Fig. 5. The curve fitting of both peaks was performed using the "Asymmetric Gaussian-Lorentzian Formula". The values of the peak intensity of both peaks (for O1s and C1s) were obtained and the oxygen-to-carbon ratio (Φ) was calculated from the following expression [61]:

$$\Phi = \frac{(I_O / S_O)}{\sum (I_j / S_j)} \qquad (1)$$

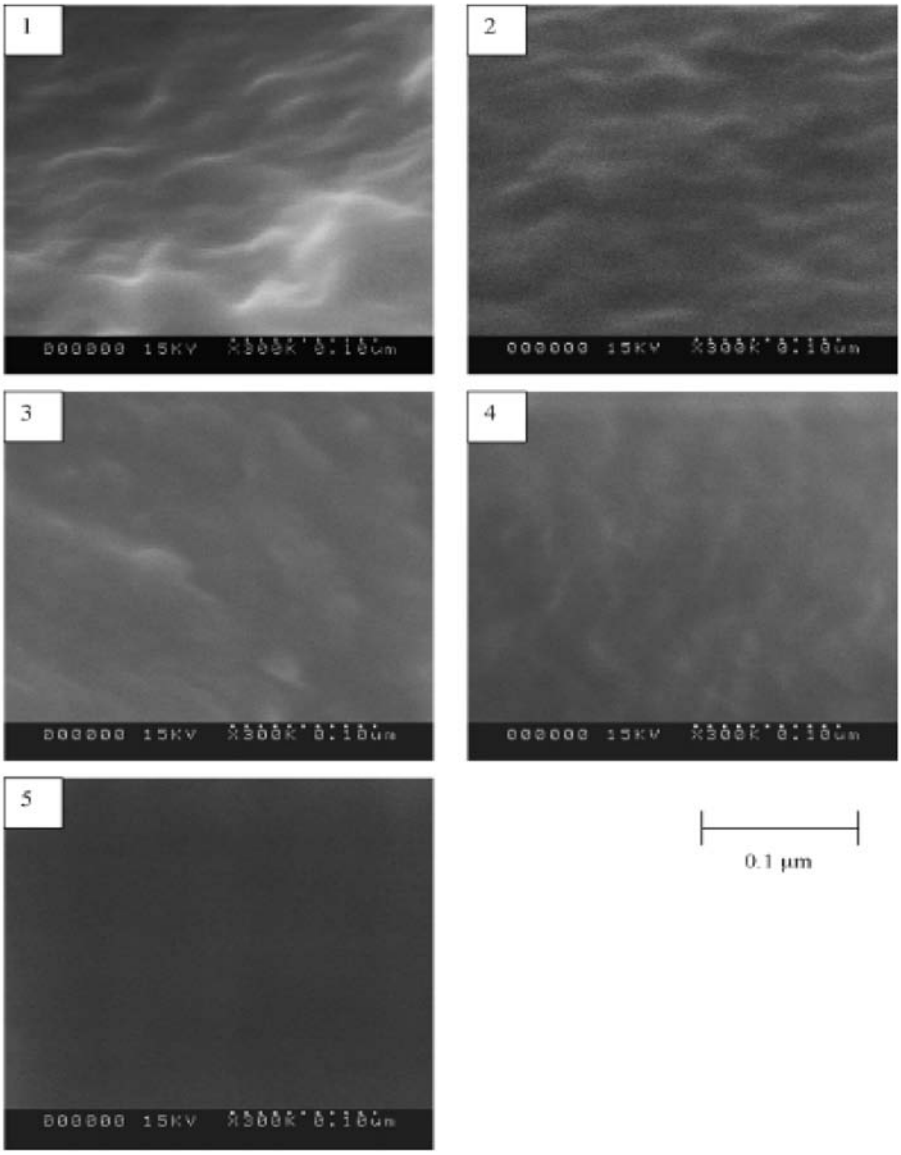

Fig. 4. SEM micrographs obtained for oxidized RVC (3.0 cm thickness) at different depth, *x* inside the electrode; 1) *x* = 0, 2) 0.5, 3) 1.0, 4) 1.5 and 5) 2.0 cm. RVC was oxidized using flow-through assembly by holding the potential at 2.0 V (Ag/AgCl) for 20 min in 0.1 M H_2SO_4 flowing at 0.08 cm s^{-1}.

where I_O and S_O are the peak intensity and the sensitivity factor for oxygen, respectively and I_j and S_j are the peak intensity and the sensitivity factor for an element j, respectively, where j is carbon and oxygen. The oxygen to carbon ratio in this case equals 0.2. This value is comparable with the reported values for untreated glassy carbon electrode [62, 63].

The distribution of the O/C ratio within the porous bed was estimated using XPS measurements for the same samples (sections) of Fig. 4. The survey spectrum of the oxidized RVC was similar to the untreated sample and the two peaks corresponding to oxygen and carbon are also revealed at same binding energies mentioned above for the untreated electrode. However, the morphology of oxygen peak does not significantly change while that of carbon is accompanied by two shoulders and one peak at high binding energies, typically at 285.2, 286.2 and 289 eV (see Fig. 6). As reported,

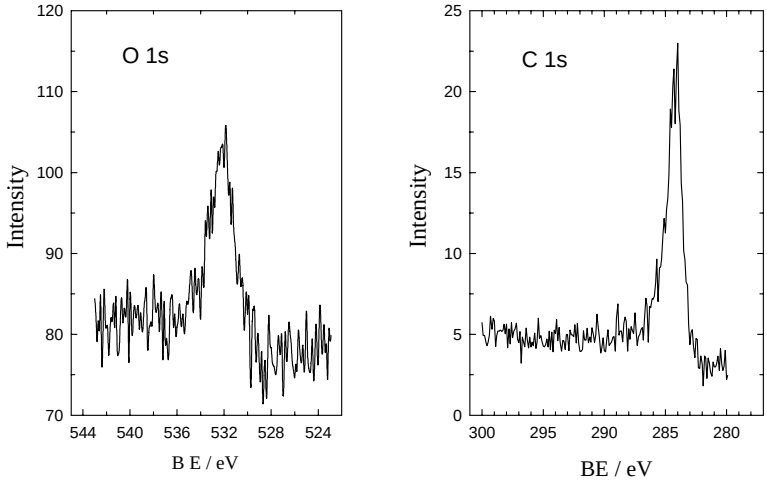

Fig. 5. C1s and O1s XPS spectra of plain (untreated) RVC.

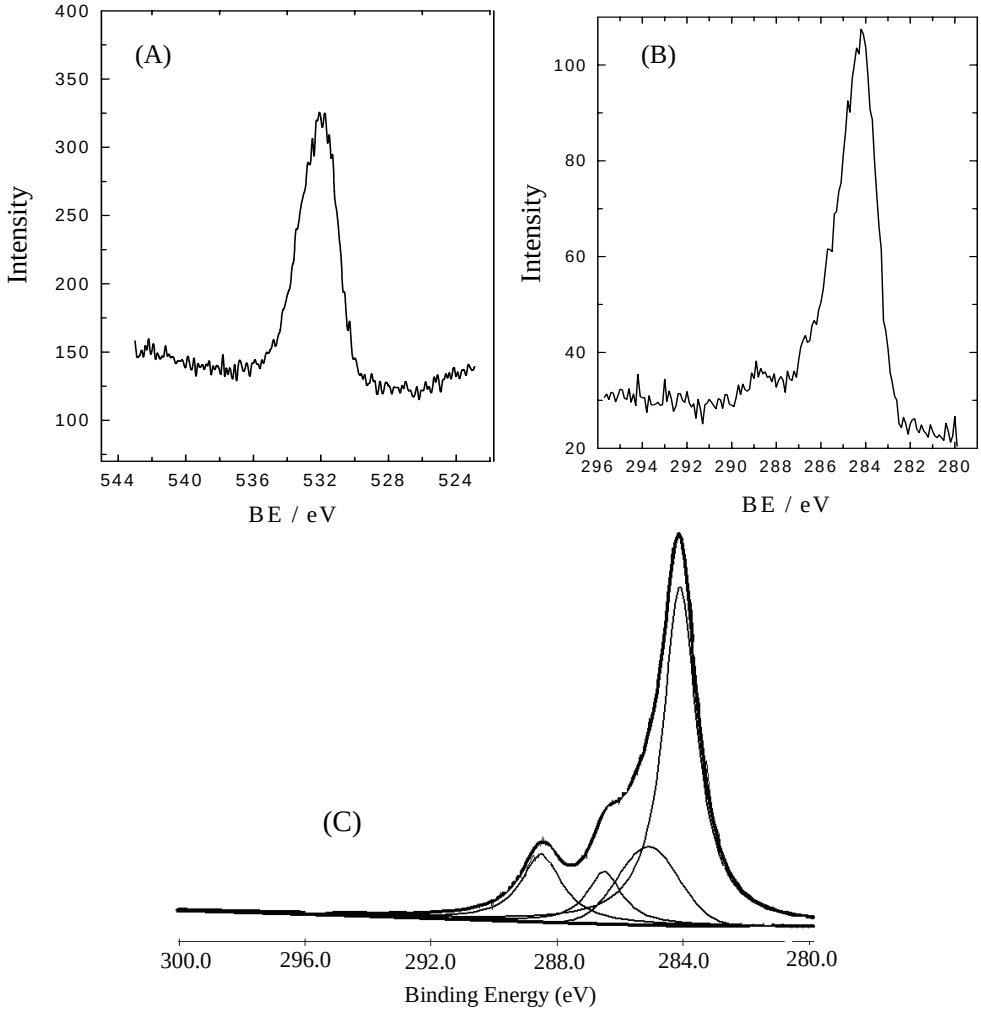

Fig. 6. C1s (A) and O1s (B) XPS spectra of oxidized RVC. (C) Curve fitting spectra of C1s of oxidized RVC.

the formed two shoulders in addition to the new peak at 289 eV correspond to the functional groups generated on electro-oxidation of the electrode [48, 64]. The peak corresponding to carbon was deconvoluted into different surface functional groups as shown in Fig. 6C. The peak at 284.2 eV is ascribed to the graphitic carbon and that at 285.2 is ascribed to a type of carbon in phenol. The peak at 286.2 eV is ascribed to carbon in carbonyl functional group and finally that at 289 eV corresponds to carbon in the carboxylic group [48]. The oxygen/carbon ratio in this case was found to increase to 0.38 as compared to the untreated RVC sample (Fig. 5). In this case oxygen to carbon ratio was calculated using the following equation:

$$\frac{O}{C} = A_{C\text{-}OH} + A_{C=O} + 2 \text{ x } A_{COOH} \quad (2)$$

where $A_{C\text{-}OH}$, $A_{C=O}$ and A_{COOH} are the intensity ratios of the different functional groups in the C_{1s} spectrum.

Fig. 7 shows the XPS spectra corresponding to oxygen taken at different depth inside the RVC electrode. The distance notation, *x* is the same as in Fig. 4 for the same samples (sections). The oxygen to carbon ratios were calculated based on Eq. 2 and its change with the depth inside the RVC electrode is given in Fig. 8. The O/C ratio decreases with the depth inside the electrode down to a value of 0.21 which is very close to the value (0.2) of the plain (untreated) electrode. This indicates the non-uniform distribution of the potential within the porous electrode. It can be concluded that around one half of the electrode is utilized in the oxidation process. These results confirm the conclusion extracted from the SEM results shown above. It is noteworthy to mention that we can obtain different distributions of the O/C ratios within the porous electrode by proper control of the anodic oxidation conditions.

4. Electrochemical hydrogen evolution reaction (HER)

Hydrogen and hydrogen energy are important issues for the current scientific literatures both for its technological and academic importance. Storage of energy in a form of hydrogen and using of hydrogen gas for direct energy conversion devices such as fuels cells represents a core for the energy future. The advantage of hydrogen energy is the

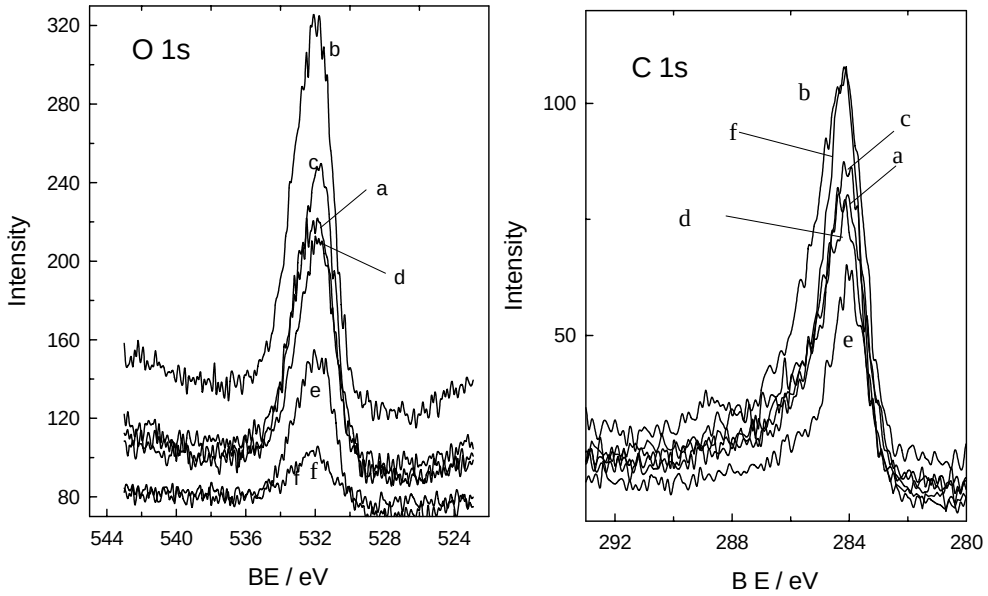

Fig. 7. C1s and O1s XPS spectra of oxidized RVC (3.0 cm thickness) taken at different depth, *x* inside the electrode; a) *x* = 0, b) 0.5, c)1.0, d) 1.5 and e) 2.0 cm. The (f) spectrum is the XPS spectrum of the plain RVC. RVC electrode was oxidized and sliced as mentioned in Fig. 4.

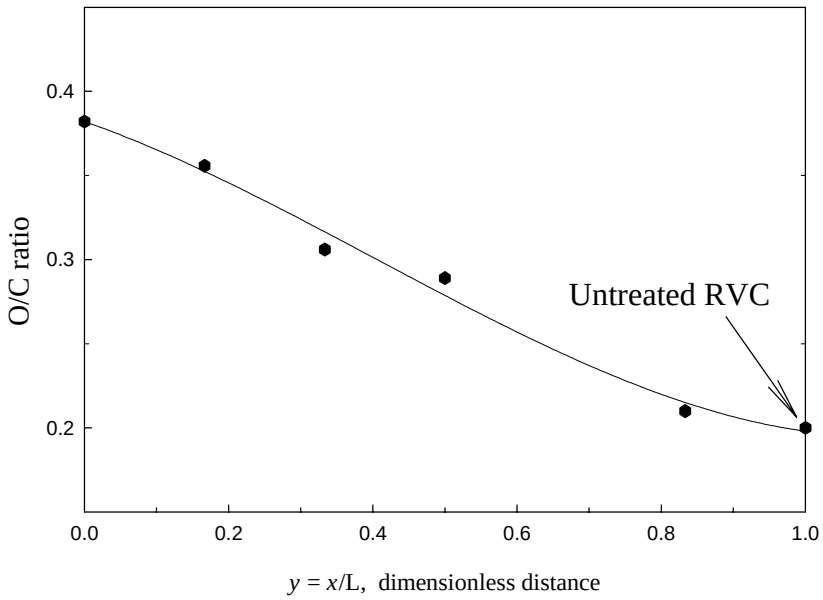

Fig. 8. The relation between oxygen to carbon (O/C) ratio and the dimensionless distance, *y* inside the electrode.

high power output, high efficiency and zero emission of pollutants. Those factors drove the world attention to the hydrogen energy as a strong candidate for replacing ordinary power sources. The electrochemical production of H_2 represents an important and main source for H_2 gas of a high purity. Hydrogen is important both for industry and energy storage applications. The development of reliable and cost effective technologies for the production of pure hydrogen is a challenging issue from electrochemical engineering point of view. For instance, for the H_2/O_2 PEM fuel, ultra pure hydrogen gas (as a fuel) is a pre-requisite. Most important conditions to fulfill good catalyst conditions are; high electrocatalysis, high stability and chemical availability of the electrocatalyst. Pure hydrogen represents a main product which is consumed in many industries. It is a key reactant needed to produce commonplace chemicals such as ammonia. The petrochemical industry uses hydrogen gas to process common fossil fuels, upgrading them to purer forms. Many electrode materials have been used for the electrochemical production of hydrogen. Those include metal, bimetallic and conducting polymer-metals composites electrocatalysts. Carbon electrode is not good candidate for HER and yet needs modifications with metals such as Ni, Ag, Au or Cu to increase its electrocatalytic properties towards HER.

In our previous works [65, 66], the hydrogen evolution reaction was studied at different type of metal loadings onto RVC matrix in alkaline medium. Copper and nickel were used and the results of HER were compared to the planar GC electrode. A mathematical model was developed to simulate the HER on GCE and the system was optimized and important kinetic parameters such as exchange current densities of HER on Cu/RVC or Ni/RVC were determined. Both planar glassy carbon and RVC were used in the measurements for comparison. The RVC was used in a flow-through porous electrode design where the electrolyte (alkaline) was forced to flow through the electrode (see Fig. 2). This is an advantage since the evolving gas bubbles are swept out of the pores resulting in a lower polarization and hence lower power consumption. Nickel metal is currently used as a cathode for water electrolyzers, and different procedures were introduced to prepare nickel electrodes with high specific surface areas. These include sintering micro porous nickel [67] production of nanoporous Raney-Nickel [68] and incorporation of Ni into PolyHIPE (high internal phase emulsions) polymer (PHP) matrix [69]. Three-phase (solid-liquid-gas) porous electrodes could be a special category of porous electrodes in which several operating parameters inherently control the overall performance of electrodes.

Of particular importance, the gas bubbles that are evolved accumulate inside the porous matrix resulting in non-uniform distributions of potential and current and, hence, in a lower effectiveness factor of the porous electrode [70]. Optimizing the electrolyte flow rate by other structural and transport parameters plays an important role in maximizing the performance of three-phase porous electrodes. Mathematical modeling can help to simulate the effects of different operating parameters on such systems.

Reticulated vitreous carbon (RVC) electrodes have been used as possible porous cathodes, operating in flow-through mode for the purpose of the electrolytic generation of hydrogen gas from flowing alkaline solutions. The electrocatalytic performance of the RVC cathode was tested under different operating conditions, such as electrolyte flow regimes and temperature. Also, the effect of electroplating the RVC with copper metal or Watts nickel in flowing electrolytes has been assessed. Potentiodynamic and galvanostatic techniques along with SEM images were used to investigate the performance of the different cathodes: bare (uncoated) RVC, copper-coated RVC (RVC/Cu), and Ni-coated RVC (RVC/Ni). Fig. 9 shows SEM images for the RVC, RVC/Ni and RVC/Cu.

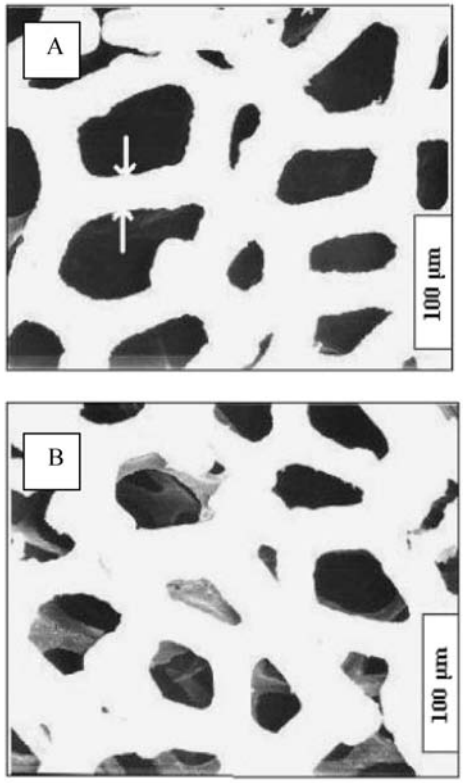

Fig. 9. SEM micrographs of the different electrodes a) bare RVC, b) RVC/Cu, and c) RVC/Ni. The white zones are the matrix. The arrows in Fig. 9a refer to a thread.

The hydrogen evolution reaction (HER) was found to be enhanced by coating RVC either with Cu or Ni. Polarization behavior had higher rates for HER using RVC/Ni than using RVC/Cu or bare RVC. Fig. 10 reveals these results. This trend was confirmed by using a planar glassy carbon electrode (GC) coated with Cu and Ni under the same conditions. The activation energies for HER using RVC and RVC/Ni were estimated to be 32 and 14 kJ mol^{-1}, respectively. Current transient and SEM micrographs showed good electrocatalytic and mechanical stability of the metal loadings. There was no indication of loss of the catalytic properties after operation for 30 h. Model calculations helped to extract kinetic parameters for the HER using different electrodes.

5. ORR and H_2O_2 production

While electrochemical reduction of oxygen via $4e^-$ path is an ultimate goal for fuel cell electrochemistry, it is not so for electrochemical production of H_2O_2. The latter needs ORR via $2e^-$ to produce H_2O_2 rather than H_2O. Hydrogen peroxide is an important chemical for many applications and uses. Here carbon electrodes can offer such conditions and yet can be used as a cathode for ORR yielding H_2O_2.

The oxidation of reticulated vitreous carbon (RVC) and its impact on the oxygen reduction reaction (ORR) in H_2SO_4 solutions has been studied. The results are compared with that of a planar glassy carbon (GC) electrode. The oxidation process was characterized by using different electrode configurations, GC (planar) and RVC electrodes both with flooded (batch process) and flow-through assembly. Cyclic voltammetry and potentiodynamic were used for the characterization of the ORR. Anodically oxidized GC and flooded RVC are similar in that the ORR on both electrodes gave a more defined limiting current plateau. Oxidation of RVC led to an enhancement of its electrocatalytic

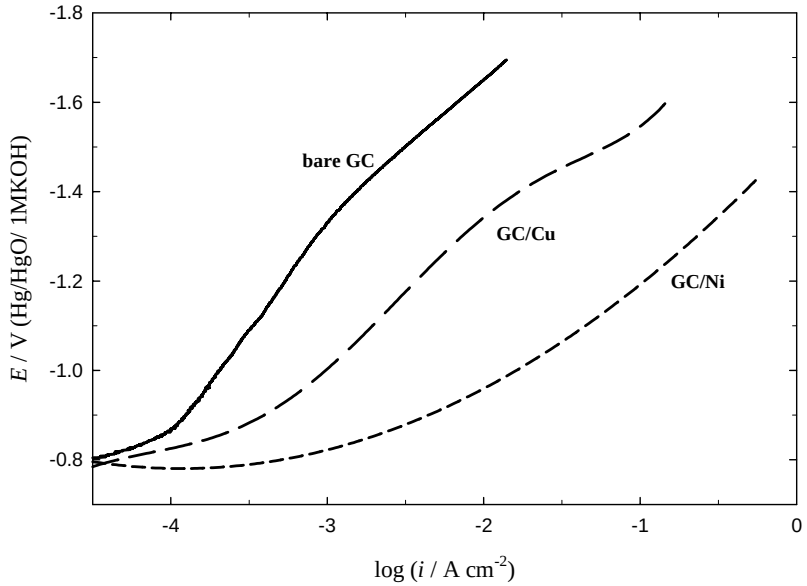

Fig. 10. *i-E* relations for HER in 2M KOH with planar GC, GC/Cu, and GC/Ni electrodes at 25°C.

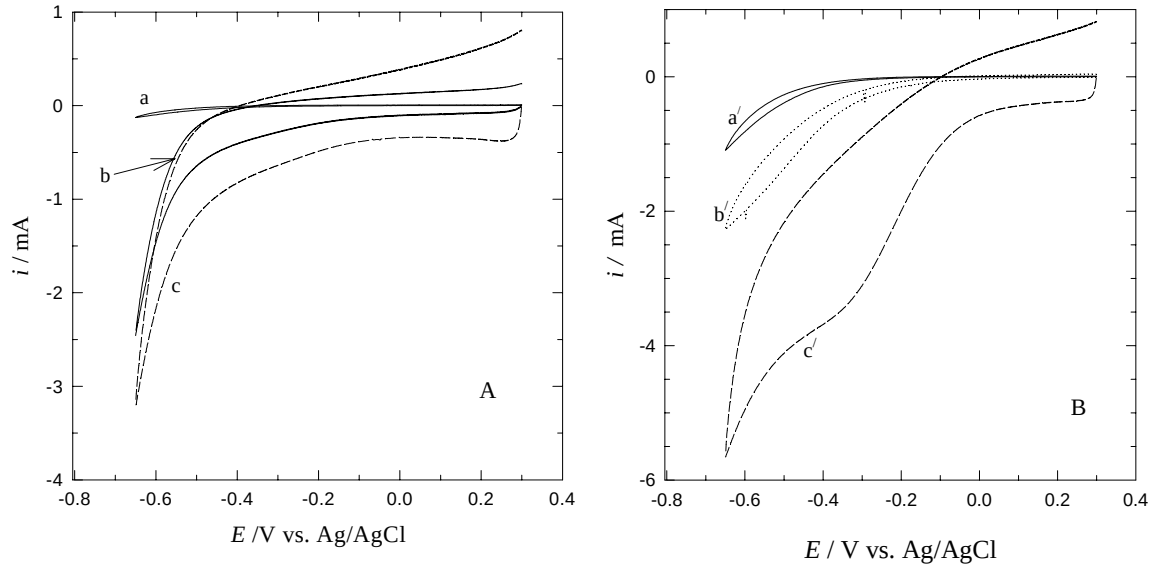

Fig. 11. CVs obtained at plain RVC (a, a/) and RVC oxidized for 1 min. (b, b/) and RVC oxidized for 5 min. (c, c/), A) O_2-free and B) O_2-staurated 0.1 M H_2SO_4 at scan rate of 20 mV s^{-1}.

properties towards ORR. H_2O_2 production was tested at the oxidized RVC from flowing acid solutions. The oxidation of RVC resulted in higher current efficiencies and higher outlet concentrations of the H_2O_2 acid solutions.

The oxidation procedure was applied to RVC electrode at stationary conditions *i.e.*, flooded assembly in 0.1 M H_2SO_4 for 1 and 5 min. Fig. 11 shows CVs for the ORR at the potential range from 0.3 to -0.7 V at the untreated and the above oxidized RVC electrodes in 0.1 M H_2SO_4. The background current at the oxidized RVC electrode is larger than that at the untreated electrode. At the oxidized RVC the oxygen reduction occurs at

more positive potentials and its current is increased. A relatively more defined limiting current plateau for ORR is observed for the RVC electrode oxidized for 5 min. (curve ć). The oxidized RVC electrode catalyzes both the ORR and hydrogen evolution reaction (HER). The hydrogen evolution enhancement is evident from the CVs recorded in the O_2-free electrolyte as shown in curves a, b and c (Fig. 11A). This can be attributed to the increase in the surface area of the RVC electrode as evident from the SEM images of Fig. 4. However, for the ORR the increase in the limiting current may be attributed to the formation of carbon-oxygen functional groups on the RVC surface (see the discussion on the XPS data). The formation of quinone functional groups on the surface of the oxidized planar GC electrode has been reported to enhance the ORR [15].

A possible confined quinone/hydroquinone redox couple can be trapped by considering the following results. GC and RVC electrodes were oxidized at 2 V for 5 min in stationary 0.1 M H_2SO_4 solution and CVs were recorded in a short potential range between 0 and 0.6 V (or 0.7 V) in O_2-free solution. Fig. 12 (A, B) shows such CVs for GC and for RVC electrodes at the same conditions and at different potential scan rates. The redox response of the quinone/hydroquinone couple at about 0.3-0.4 V is found for GC in Fig. 12A. It is distorted at the porous RVC electrode as shown in Fig. 12B. It seems from this figure that the quinine/hydroquinone couple does not mediate the oxygen reduction in the present case as the oxygen reduction is observed at far more negative potential than the redox potential of the quinone/hydroquinone couple. Similar behavior has been reported by Nagoka *et al*. [64, 71] who found that while adsorbed quinone mediates oxygen reduction, the quinone group generated by electro-oxidation of glassy carbon did not mediate it. The reason behind the catalysis of the oxygen reduction on the electrochemically pretreated electrodes is not clear. It is likely that the surface functional groups formed on the anodic oxidation of the electrode may act as preferable sites for the oxygen adsorption. The charge (Q) consumed in the hydroquinone oxidation is determined by integration of the anodic part of a CV (similar to that in Fig. 12B) of the quinone redox couple at the RVC electrodes; plain and oxidized for 1 and 5 min. These were found to be 0.0, 0.05 and 0.15 C for these electrodes, respectively. The zero charge of the plain RVC is evident from the CV of the plain RVC in Fig. 12B. Note that the charging current of the double layer (base current) was subtracted in each CV of the 1 and 5 min. oxidation. The number of surface quinone units (S) was estimated using the following equation:

$$S = \frac{NQ}{nF} \tag{3}$$

where N is the Avogadro number, n is the number of electrons involved in the quinone-hydroquinone redox reaction represented by Eq. 4:

$$Q + 2\,H^+ + 2e = QH_2 \tag{4}$$

and F is the Faraday constant. The number of active sites equals 1.4×10^{16} and 5.2×10^{17} quinone units for the oxidized RVC for 1 and 5 min, respectively. The increase of the peak current and positive shift of peak potential in Fig. 11 may be attributed to the increase of the quinone active sites.

6. Electrogeneration of H_2O_2 on oxidized RVC

H_2O_2 is an important chemical in the current technological, environmental and academic research fields [72, 73]. One of the most common materials used as a porous cathode for H_2O_2 generation is the RVC electrode [74, 75]. In most cases the electrode was used as it is or with little treatment. The activation of RVC electrodes in all of the above applications was either not mentioned at all or only reported briefly as a repetitive potential scan of the RVC electrode to obtain reproducible electrochemical measurements. Strong *et al*., [76] have recently found that the oxidation of the RVC material with a mixture of H_2SO_4 and HNO_3 significantly increased the number of carboxylic acid groups on the surface. This enabled a covalent attachment of functional groups capable of metal ion exchange. The electrochemical pretreatment effects on the electrochemical generation of H_2O_2 at flow-

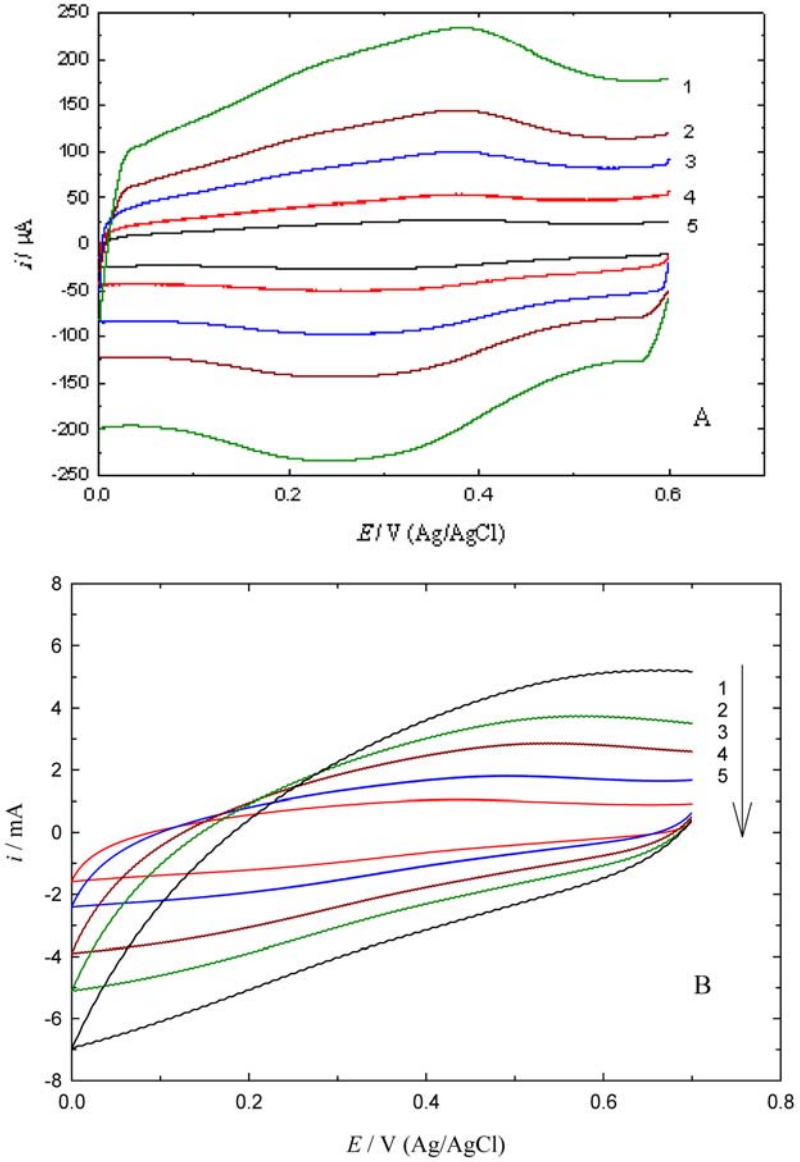

Fig. 12. CVs obtained at electro-pretreated GC (A) and RVC (B) electrodes at different scan rates in N_2-saturated 0.1 M H_2SO_4. Scan rates: (1) 50, (2) 100, (3) 200, (4) 300 and (5) 500 mVs^{-1}.

through porous electrode made of reticulated vitreous carbon are tested in comparison with those of GC electrode [40]. Do and Chen [77] studied the effects of the anodic treatment of graphite planar electrode on the electrocatalysed H_2O_2 electrogeneration. To the best of our knowledge, there is no systematic study on the anodic oxidation of RVC electrode and its effects on the electrocatalytic properties towards ORR albeit RVC electrodes have been used for many applications.

H_2O_2 is electrochemically produced via 2e reduction of oxygen as follows;

$$O_2 + 2H^+ + 2e = H_2O_2 \quad E^o = 0.682 \text{ V vs. NHE} \tag{5}$$

In acidic media, there are two possible competitive reactions during this reduction, i.e., further reduction of H_2O_2 to H_2O and hydrogen evolution reaction (HER);

$$H_2O_2 + 2H^+ + 2e = 2H_2O \quad E^o = 1.776 \text{ V vs. NHE} \tag{6}$$

$2H^+ + 2e = H_2 \qquad E^o = 0.0$ V vs. NHE (7)

The main reaction in this case is the HER since further reduction of H_2O_2 to H_2O occurs at a relatively higher negative potential [78, 79]. Figure 13 shows polarization curves for the RVC and oxidized RVC electrodes in 0.1 M H_2SO_4 flowing at 0.08 cm s^{-1}. Both ORR and HER are enhanced at the oxidized RVC electrode (see Fig. 11). No limiting current plateau was observed at both electrodes due to ohmic drop within the electrode bed [80]. H_2O_2 was electrochemically produced at the plain RVC and compared with that obtained at the oxidized RVC (RVC was oxidized by applying a constant potential of 2.0 V in 0.1 M H_2SO_4 for 5 min). The electrogeneration of H_2O_2 was conducted using accumulation set up, i.e., a given volume of O_2-saturated H_2SO_4 was circulated over the RVC bed electrode at a suitable flow rate. The flow rate of 0.28 cm s^{-1} was used to enable an efficient recirculation of the electrolyte. The outlet stream was recirculated for a period of 10 min. The absence of further reduction of H_2O_2 to H_2O in the present condition may enable the production of H_2O_2 of high concentration on accumulation. It has been reported that under similar conditions H_2O_2 is not reduced at more positive potential than -1.0 V [78, 79]. The current efficiency of H_2O_2 electrogeneration after accumulation, *CE*% can be given as;

$$CE\ \% = \left[\frac{2\,F\,C_{H_2O_2}\,V}{i_{cell}\,t}\right]100 \qquad (8)$$

where $C_{H_2O_2}$ is the H_2O_2 concentration in the outlet stream in mol cm^{-3}, V is the volume (cm^3) of the electrolyzed solution, i_{cell} is the observed current in ampere and t is the time of operation in s. Fig. 14 shows the effect of applied potential on the current efficiency of H_2O_2 obtained at the plain RVC (curve a), and oxidized RVC (curve b) electrodes. At the oxidized RVC electrode, the current efficiency of 100% was obtained at a potential as positive as -0.2 V and decreased as the applied potential was increased negatively. At higher negative potentials the HER becomes a

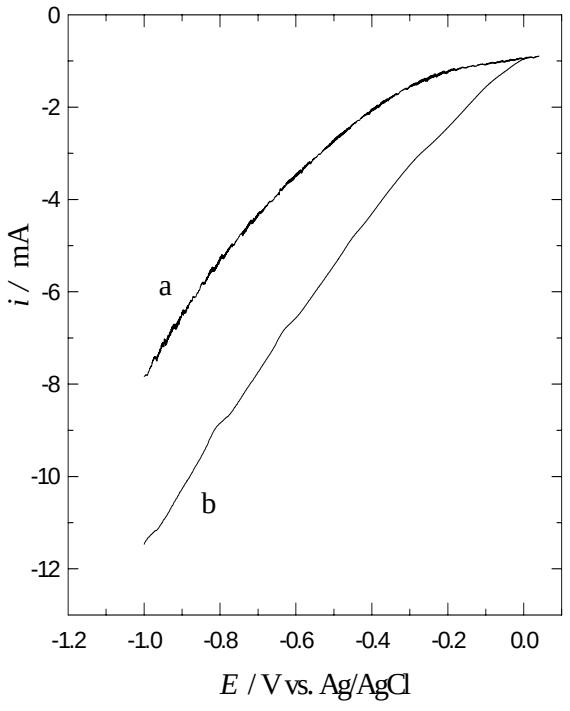

Fig. 13. Polarization curves for plain RVC (a) and oxidized RVC (the electrode was oxidized for 5 min); (b) electrodes in 0.1 M H_2SO_4 flowing at 0.08 cm s^{-1}. Potential scan rate: 10 mVs^{-1}.

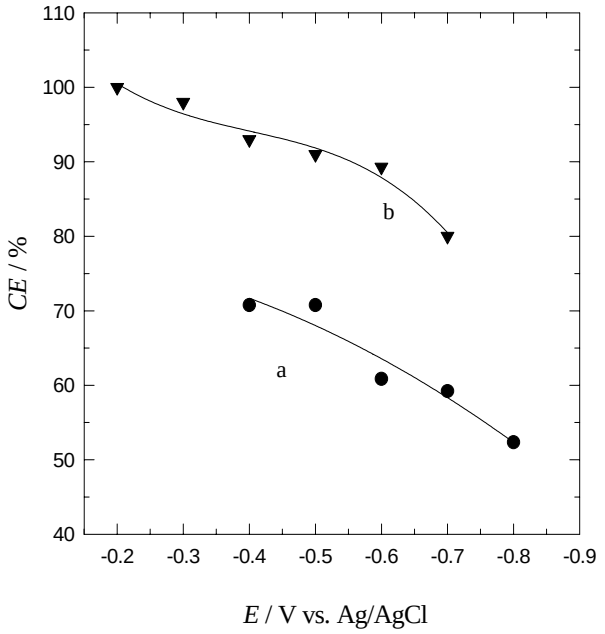

Fig. 14. Current efficiency of H_2O_2 electrogeneration at plain RVC (a); and oxidized RVC (b) at different potentials using 0.1M H_2SO_4 solution flowing at 0.28 cm s^{-1}.

competing reaction with the ORR and the CE% decreases with the potential.

The effect of applied potential on the concentration of the produced H_2O_2 is shown in Table 1. As the potential increases negatively, the concentration of H_2O_2 increases in the examined potential range. That is to say, the higher rates of the ORR (higher currents) obtained at more negative potential are overweighing the decrease in *CE*%. The increase in current is more pronounced than loss in current efficiency. The increase in concentration of the produced H_2O_2 with the applied potential indicates an insignificant reduction of H_2O_2 to H_2O at this potential range.

The anodic oxidation of RVC resulted in the electrocatalysis of the oxygen reduction and consequently the generation of H_2O_2 at lower negative potentials than at the untreated electrode. This was reflected on the higher current efficiency obtained at the oxidized RVC. This point can be formulated suitably by calculating the energy saving, $\Delta\xi$ (at a certain electrode potential E) by the following equation;

$$\Delta\xi = \xi_{\text{bare}} - \xi_{\text{ox}} \tag{9}$$

where ξ_{plain} and ξ_{ox} are the specific energy consumption in kWh per kg of H_2O_2 at the plain and the oxidized RVC, respectively. The specific energy consumption, ξ can be generally given by;

$$\xi = \frac{i_{\text{cell}} E_{\text{cell}}\, t}{3600\ m} \tag{10}$$

where E_{cell} is the measured cell voltage in volt and m is the mass of H_2O_2 in g produced in time, t (second). Eqs. 9 and 10 were applied to estimate the energy saving, $\Delta\xi$ at different electrode potentials. Table 1 shows the energy saving obtained at different potentials. In general, the energy saving increases with the electrode potential until it reaches a constant value. The difference in the cell currents at the plain and the oxidized RVC electrodes increases with the electrode potential (see Fig. 14). As the cell current increases, the rate of the electrochemical reaction (current) increases and also the amount of the produced H_2O_2 increases. A combination of the above effects results in the obtainable energy saving. At highly negative electrode potentials, however, the rate of the hydrogen evolution reaction becomes significant and no further energy saving is obtained beyond potentials more negative than -0.6 V. It is obvious that an energy saving is gained as a result of the anodic oxidation process, which should be considered for applications of RVC.

7. Oxygen evolution at modified GCE

In this section the recent applications of manganese oxide (MnO_x) modified GCE in oxygen evolution will be summarized. MnO_x is characterized by its natural abundance and low cost and its environmental compatibility in addition to its unique electrocatalytic properties, and thus it has made it one of the most promising electrode materials for many applications. Mn oxides are commonly prepared by co-precipitation [80, 81], thermal decomposition [82], physical vapor deposition [83], sol-gel processes [84, 85], hydrothermal synthesis [86], and electrochemical methods [87-95].

Table 1. Effect of applied potential on $C_{H_2O_2}$ and power saving, $\Delta\zeta$, (kWh per kg H_2O_2).

Applied potential / V	$C_{H_2O_2}$ / μM		$\Delta\zeta$ / (kWh per kg H_2O_2)
	Bare RVC	Oxidized RVC	
-0.3	27.5	52.5	1.0
-0.4	22.5	57.5	2.2
-0.5	47.5	72.5	3.6
-0.6	62.5	102.5	3.0
-0.7	62.5	102.5	2.9

Developing of non-noble metal catalysts for oxygen evolution and reduction is of interest for fuel cells that use alkaline electrolyte solutions. Among these electrocatalysts MnO_x is one of the most promising catalyst for this purpose [95-99]. Oxygen evolution reaction (OER) plays a prominent role in electrochemical science and technology as it is inherently involved in many vital applications, e.g., energy conversion and energy storage devices [100]. It couples many of the cathodic processes occurring in aqueous solutions such as water electrolysis. It is considered as the main source of overpotential in the industrial water electrolysis processes. Thus, a great interest is directed to the catalyst of this reaction for developing of a low-overpotential oxygen evolution anode which has a prime importance in electrochemical technology. Water electrolysis is traditionally carried out in alkaline media for the production of highly pure hydrogen gas [101-105]. Alkaline media are preferred because of the less susceptibility of the anode to corrosion problems and thus cheaper materials with long life time can be used as efficient anodes [106, 107]. Some metal oxide-based electrodes have been reported to catalyze the OER. Among them Ni and Co oxides have been extensively studied [108-115]. Various Mn oxides have been also reported to catalyze the OER; the extent of catalysis is based on the synthesis method of the electrode as well as on the nature of the dopant such as Mo or W [116-119].

7.1. Preparation and characterization

MnO_x nanoparticles (nano-MnOx) were electrodeposited onto GCE from a solution containing 0.1 M Na_2SO_4 + 0.1 M $Mn(CH_3COO)_2$ via cycling the potential between 0.0 and 0.4 V vs. Ag/AgCl/KCl(sat) at 20 mV s^{-1} [99]. The SEM of the thus prepared nano-MnOx/GC is shown in Fig. 15. The MnO_x was electrodeposited homogeneously on the entire surface of the GC electrode in a porous texture, which enables the accessibility of the solution species to the underlying substrate through nano channels across the MnO_x nanotexture. The electrodeposited nano-MnOx/GC has been characterized using XRD and XPS [92, 93]. X-ray photoelectron spectroscopy (XPS) results proved the effective deposition of nano-MnO_x on GC [93]. The X-ray diffraction

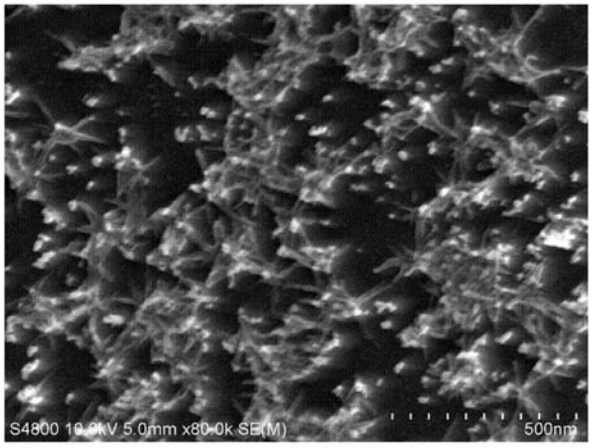

Fig. 15. SEM images of the nano-MnO_x modified GC electrode. The nano-MnO_x was electrochemically deposited from an aqueous solution of 0.1 M Na_2SO_4 containing 0.1 M $Mn(CH_3COO)_2$ by applying 50 potential cycles between 0 and 0.4 V vs. Ag/AgCl/KCl (sat.) at potential scan rate of 20 mV s^{-1}.

(XRD) pattern of the MnO_x modified electrode revealed characteristic peaks of the manganite (manganese oxide hydroxide, γ-MnOOH) phase appeared at 2θ = 26.58°, i.e, indicating the electrodeposition of MnO_x in a single crystalline phase [92, 93].

7.2. Electrochemical measurements

Figure 16 shows the CV response measured in N_2-saturated 0.5 M H_2SO_4 at (a) bare and (b) modified GC electrode. The MnO_x possesses some sort of electrochemical activity as revealed from the broad (rather small) reduction peak located at ca. 1.1-1.2 V [89]. The following redox reaction may account for the observed redox response [120-122]:

$$MnO_2 + H^+ + e^- \rightarrow MnOOH \qquad (11)$$

This reaction involves a reversible proton insertion process in acidic media concurrently with a reversible change of the oxidation state from Mn(IV) to Mn(III) [123].

Fig. 17 shows linear scan voltammograms (LSV) for the oxygen evolution reaction (OER) measured in N_2-stuarated 0.5 M KOH solution at (a) bare and (b) nano-MnOx modified GC electrodes. This figure shows a significant enhancement of the polarization behavior of the GC upon modification with nano-MnOx; around

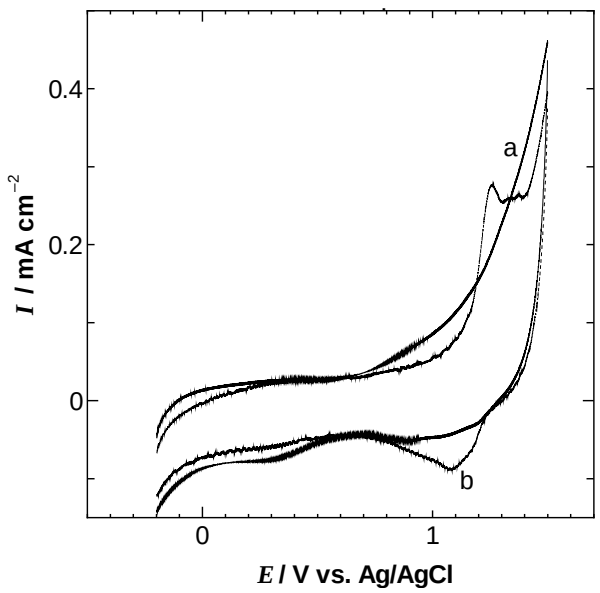

Fig. 16. CVs response obtained at (a) bare and (b) nano-MnO_x modified GC electrode in N_2-saturated 0.5 M H_2SO_4 at potential scan rate of 100 mV s^{-1}. The nano-MnO_x modified electrodes were prepared as mentioned in the caption of Fig. 15.

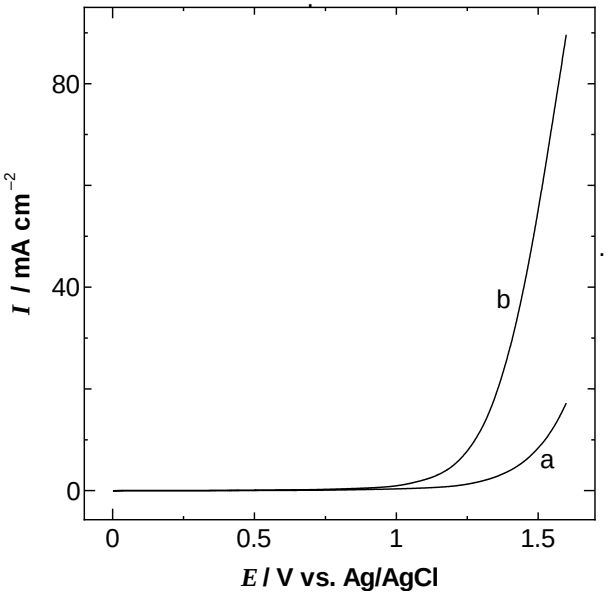

Fig. 17. LSV for the OER in N_2-saturated 0.5 M KOH at (a) bare and (b) nano-MnOx/GC electrode at potential scan rate of 20 mV s^{-1}. The nano-MnO_x modified electrodes were prepared as mentioned in the caption of Fig. 15.

300 mV negative shift in the onset potential of the oxygen evolution is observed.

7.3. Origin of the electrocatalytic enhancement

The OER is an anodic process which takes place at most of the metal electrode surfaces at potentials sufficiently anodic to allow for the formation of various kinds of oxides. Some of these oxides are known to enhance the OER, e.g., nickel oxide in the β-phase (i.e., NiOOH) [124, 125]. This oxide is thought to participate in the reaction mechanism in such a way that facilitates the charge transfer. In the current study the electrodeposited manganese oxide (γ-MnOOH) is of an isomorphous structure to NiOOH and thus is likely to function similarly towards the OER in alkaline media. Thus, the following mechanism was suggested for the observed enhancement of the OER [91, 124].

$$OH^- \rightarrow (OH)_{ads} + e^- \quad (12)$$

$$(OH)_{ads} + OH^- \rightarrow (O^-)_{ads} + H_2O \quad (13)$$

$$(O^-)_{ads} \rightarrow (O)_{ads} + e^- \quad (14)$$

And finally

$$2\,(O)_{ads} \rightarrow O_{2(gas)} \quad (15)$$

γ-MnOOH phase has been proposed to be involved in one (or more) of the above steps according to:

$$2\,\gamma\text{-MnOOH} + (O^-)_{ads} \rightarrow 2\,MnO_2 + H_2O + e^- \quad (16)$$

$$MnO_2 + (OH)_{ads} \rightarrow \gamma\text{-MnOOH} + (O)_{ads} \quad (17)$$

where the subscript term “ads” refers to surface adsorbed species.

8. Ozone electrogeneration

In this part the ozone electrogeneration at carbon electrodes will be reviewed with special attention to our recent work in this area. In the previous section the oxygen evolution catalysis is mentioned. In fact for an electrode to be suitable for ozone electrogeneration it should be not active for oxygen evolution. Ozone (O_3) is the candidate for the application of advanced oxidation technology which involves the hybrid use of several oxidants at the same time. It is the first choice for better oxidation performance both from environmental and technological points of view [126, 127], and for achieving a high purification standard of drinking water [128-132].

Generally, there are two methods for the generation of O_3, the electrochemical and the corona methods. The former leads the latter one as it generates O_3 at higher current efficiencies and it enables on-site applications of O_3 which is a remedial for the instability of O_3 [133-137].

The electrogeneration of O_3 at high current efficiency is of prime importance [133, 138-162] for forcing the application of O_3 in many fields such as water drinking, silicon wafer cleaning in semiconductor device manufacturing, wood pulp bleaching, combustion of resistant organic pollutants, and clean-up of effluents pushing the development of a chlorine-free technology [163-169]. The selection of a suitable anode for electrogeneration of O_3 is the main challenge. Several electrodes such as the costly Pt [155, 170], glassy carbon [71], boron-doped diamond [159] and lead oxide [146, 171-177] have been used for O_3 electrogeneration. An efficient electrode for the electro-generation of O_3 is the one that fulfills the most important requirements; that is impeding the oxygen evolution, which is thermodynamically favorable over O_3 evolution (see Eqs. 18 and 19) and achieving the stability terms.

$$O_2 + 4H^+ + 4e = 2\ H_2O \qquad E^o = 1.23\ V \qquad (18)$$

$$O_3 + 6H^+ + 6e = 3\ H_2O \qquad E^o = 1.51\ V \qquad (19)$$

Carbon electrodes have been reported to be inactive for O_3 evolution under common experimental conditions due to its instability for the severe environment formed in the anode compartment. The latter includes the formation of strong oxidant, applying a high anodic potential for generation of O_3, and operating at low pH in the anodic compartment [146]. Under special conditions of very low temperature and in the presence of fluoride-containing electrolytes, glassy carbon electrode (GCE) has been proved to be an efficient O_3 generator with a high current efficiency of 62% at -5°C [133]. The modification of the adsorbability of the O_2 intermediate in presence of fluoride anion increases the O_3 yield [146]. Using low temperature is also important in increasing the yield as decreasing temperature generally increases O_3 yield via inhibiting O_2 electrochemical evolution and decreasing the continuous decomposition of O_3 which is significant at room temperature [158, 163]. However, using such drastic conditions is not facile for practical applications. Among noble metals, a platinum electrode is considered to be the candidate favorable for retarding O_2-evolution [178, 179], and it has been also reported to produce high current efficiency for the generation of O_3 at low temperatures, e.g., -63.5°C [146, 180]. This efficiency significantly decreases upon increasing temperature to room temperature [146, 180].

Electrogeneration of O_3 has been also studied at porous electrodes, especially flow-through porous electrode [181, 182]. Flowing electrolyte or continuous process has advantages over batch process as it gives a continuous feed of the dissolved products. Three-dimensional electrodes made of RVC have diverse applications especially when they operate as flow reactors [5, 183]. They have been suggested for waste water treatments [184, 185] and removal of heavy metal ions from dilute streams [56, 185, 186]. The combination of the properties of Pt and RVC resulted in a suitable arrangement for O_3 generation using stationary and flowing H_2SO_4 solutions has been reported [182]. Kraft *et al*. [187] used diamond planer electrode for the electrogeneration of O_3 from flowing solutions. Operating porous electrode in a flow regime offers many merits such as sweeping out the gas bubbles. Accumulation of gas bubbles deteriorates the overall performance of the porous electrode and affects the polarization and current distributions within the porous electrode [66, 188, 189]. In addition, using continuous feeding of O_3 aqueous solutions could solve the problem of continuous decomposition of O_3.

8.1. Electrogeneration of ozone at flooded RVC

The electrogeneration of O_3 at RVC/Pt electrode both in flooded and flow regimes has been reported [181]. In case of flooded electrode the electrogeneration of O_3 at a constant potential of 4.0 V applied for 5 min was increased from 0.2% at bare RVC to 1.6% at RVC/Pt electrode. This value is more than twice the reported value at the planar platinum electrode [136].

8.2. Electrogeneration of ozone at flow-through RVC

8.2.1. Effect of potential

The electrogeneration of O_3 using a flow-through regime arrangement produces a continuous feeding

of O_3-containing streams. Several parameters have been studied including the effect of acid concentration, flow rate and potential. The current efficiency and power saving for O_3 electrogeneration at different applied anodic potential in the potential range from 2 to 4 V are shown in Table 2. The lower limit of this potential range (2.0 V) was selected to be higher than the thermodynamic potential of the O_3 evolution and the upper limit (4.0 V) to test the performance of the electrode at a relatively high potential. The current efficiency (*CE*%) per single pass was determined from Eq. 8. Specific electrical energy consumption (*SE*) in kWh per kg of O_3 was determined by Eq. 10. The data in Table 2 reveals that the highest current efficiency is obtained at potential around 3.0 V. The concentration obtained at 3.0 V was also comparable to that obtained at higher potentials. At the same time, a much lower specific energy consumption compared to that at higher potentials was obtained.

8.2.2. Effect of acid concentration

The effect of acid concentration on the electrogeneration efficiency of O_3 and the specific energy consumption at different acid concentrations at a specific electrode potential holding the potential for 5 min and at a specific flow rate is shown in Fig. 18. The current efficiency is shown in the inset at the same conditions. The current efficiency was not significantly changed with increasing the acid concentration (inset). As the acid concentration increases the C_{O3} increases and the specific energy decreases. However, using a high concentration of acid may result in a new competition reaction (persulfate formation) with O_3-evolution in addition to the unavoidable oxygen evolution. The decrease in *SE* is due to the decrease in the cell voltage upon increasing the electrolyte concentration. Minimum specific electrical energy consumption at a C_{acid} 1.0 M was obtained.

8.2.3. Effect of flow rate

Figure 19 shows the relationship between the O_3 concentration in the outlet solution and the flow rate obtained at an applied potential of 3.0 and 4.0 V in 0.1 M H_2SO_4. The outlet concentration of O_3 increased with the decrease in flow rate. As the flow rate decreases, the residence time increases leading to the increase in the concentration of O_3 in the outlet effluent solution. At a certain flow rate, the C_{O3} obtained at 4.0 V is higher than that obtained at 3.0 V even though the current efficiency at 3.0 V is higher than that at 4.0 V. This could be understood from the high current sustained, i.e., higher electrochemical rate of O_3 generation at 4.0 V in comparison with that at 3.0 V. This may outweigh the higher current efficiency obtained at 3.0 V. A desired O_3 concentration may be obtained at a specific flow rate using a flow-through porous electrode, because not only the electrochemical parameters but also the hydrodynamic parameters affect the product concentration.

8.2.4. Stability of the electrode

The stability of RVC/Pt electrodes has been tested by recording the current-time relation at a specific electrode potential. When the electrolysis was carried out in 0.1 M H_2SO_4 at 4.0 V, for the flooded RVC/Pt electrode the current decreased from 73 to 60 mA cm^{-2} for an operation period of 2 h. The current efficiency decreased from 1.6 to 1.2% during this period. On the other hand, for the flow-through porous electrode a constant current of 80 mA cm^{-2} was obtained for about 20 h in 0.1 M H_2SO_4 at 3.0 V. The current efficiency

Table 2. Current efficiency, ozone concentration, and specific energy consumption obtained at different applied potentials.

Applied potential /V	% *CE*	$[O_3]$ / μM	*SE* (kWh kg^{-1} O_3 x 10^3)
2.0	1.6	5	0.75
2.5	1.9	10	1.06
3.0	2.2	24	1.37
3.5	1.8	23	2.18
4.0	1.5	25	3.01

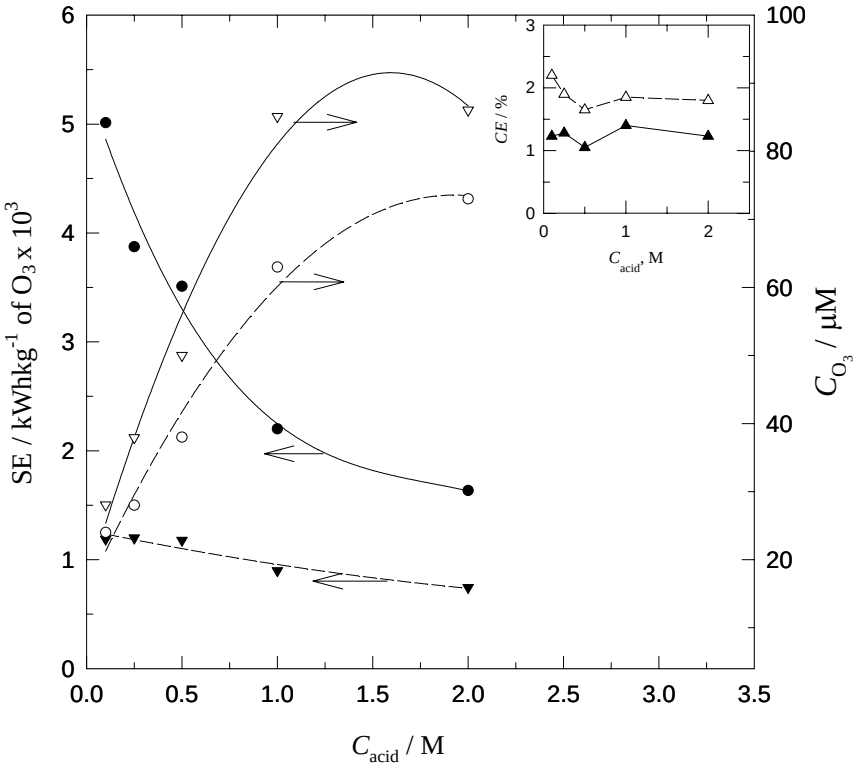

Fig. 18. Effect of C_{acid} and electrode potential on the concentration of the generated O_3 and specific energy at RVC/Pt electrode using flow rate of 0.08 cm s^{-1}. Inset shows the current efficiency of O_3 generation at different acid concentrations. Applied electrode potentials: (- - -) 3.0 and (—) 4.0 V.

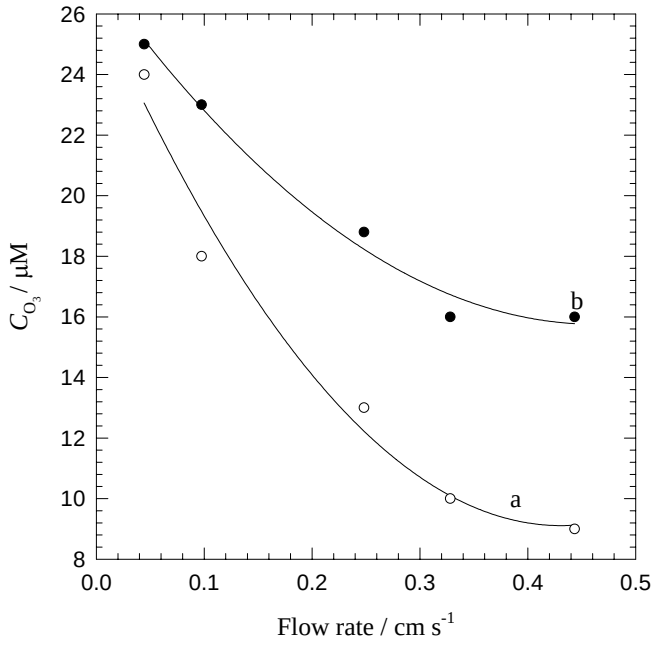

Fig. 19. Effect of flow rate on C_{O3} at flow-through porous RVC/Pt electrode using applied potential of (a) 3 and (b) 4 V in 0.1 M H_2SO_4 and at 25°C.

remained constant during this period (*CE* = 2.2%). However, the *CE*% decreased to a lower value after this period. The faster loss of the current efficiency at the flooded electrode may be attributed to the electroplating procedure of Pt. At the flooded electrode, a stationary electrolyte containing H_2PtCl_6 was used, while a flowing-electrolyte was used at flow-through porous electrode. In the latter case, a more uniform and effective deposition of Pt onto the RVC matrix may be guaranteed while in the former case the deposition takes place only on the external surface of the RVC matrix. At the flooded electrode the Pt was easy to be flaked off from the matrix. This point can be confirmed by studying the SEM in Fig. 20 in which the SEMs of the RVC/Pt were taken before (image a) and after (image b) being used for the electrolysis of 2 h. A considerable fraction of the surface Pt flaked off as shown in image b. This may help to understand the significant decrease in the current efficiency after the electrolysis at the flooded electrode. A similar conclusion can be driven to rationalize the loss of the efficiency of the flow-through porous electrode.

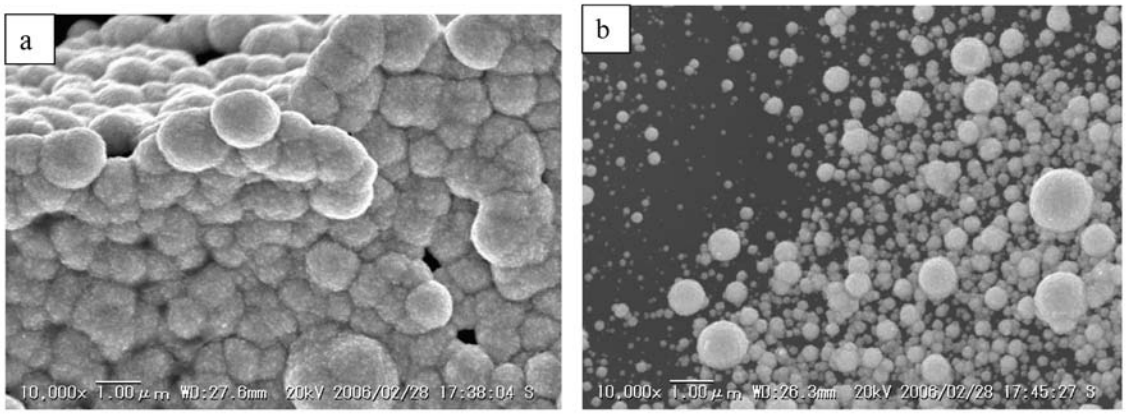

Fig. 20. SEMs for RVC/Pt (a) before and (b) after being used for electrolysis of 2 h at flooded RVC electrode at 25°C. Pt was deposited from stationary 0.1 M H_2SO_4 solution containing 5 mM platinate by applying a constant potential of 0.0 V vs Ag/AgCl for 1 h.

Table 3. Some literature values for the electrogeneration efficiency of O_3 at different electrodes and experimental conditions.

Electrode	Temp. (°C)	Electrolyte	Current density (A/cm^2)	Efficiency (%)	Reference
β-PbO_2	RT	1 M Na_2SO_4	0.4	5.1	190
	20	3 M H_2SO_4 + KPF_6	0.8	< 6	136
	10	phosphate buffer (pH 7.5)	0.2	6.1	191
	0.0	5 M H_2SO_4	0.6	< 8	176
Pt	-63.5	3.25 M H_2SO_4	0.75	32.4	192
	0.0	3.25 M H_2SO_4	0.75	1-2	193
	25	11 M $HClO_4$		0	
Ti/RuO_2	0	5 M H_2SO_4	0.4 -1.4	0	147
Au, Pd	0	5 M H_2SO_4	0.4 -1.4	0	146
Sb-Ni doped SnO_2	0	0.1 M H_2SO_4	*E* = 2.2 V	36.3	194
Ti/IrO_2-Nb_2O_5	RT	3 M H_2SO_4 + 30 mM KPF_6	0.2 -1.4	12	193

Table 3 summarizes some of the reported values for the current efficiencies of O_3-electrogeneration obtained at different electrodes under various experimental conditions with that obtained at the RVC/Pt electrode. Usually, the generation of O_3 is carried out at very low temperature (0°C or lower) and in the presence of very high concentrated acidic medium as it is reported that the oxygen overvoltage increases with decreasing temperature and pH [162, 163]. Supporting electrolyte-containing F^- has been reported to give the high current efficiency as compared with those not containing F^-. This has been attributed also to the increase of the oxygen overvoltage in the presence of F^- [146]. Foller and Tobias reported that on adding F^- to 3.5 M H_2SO_4, the anode potential of β-PbO_2 electrode shifted to high positive potential and this was reflected in the doubling of the ozone current efficiency [146]. However, electrogeneration of O_3 under drastic conditions of high acidity and in the presence of F^- limits the applications of O_3 as it decreases the endurance of the electrode and contaminates the O_3 solution with the corrosive F^-. In addition, the generation of O_3 at very low temperature is another economical limitation.

ACKNOWLEDGEMENTS

The present work was financially supported by Grant-in-Aid for Scientific Research (A) (No.19206079) to T. Ohsaka, from the Ministry of Education, Culture, Sports, Science and Technology, Japan.

REFERENCES

1. Walker, P. L. and Radovic, L. R. Chemistry and Physics of Carbon; Dekker: New York.
2. Kinoshita, K. Carbon, Electrochemical and Physicochemical Properties; John Wiley and Sons: New York, 1988.
3. McCreery, R. L. Electroanalytical Chemistry; Bard, A. J. 1991, Ed.; Dekker, New York, Vol. 17.
4. Leon, Y. C. A. and Radovic, L. R. 1994, Chemistry and Physics of Carbon; Thrower, P. A., Ed.; Dekker: New York, Vol. 24.
5. Friedrich, J. M., Poncede-Leon, C., Reade, G. W. and Walsh, F. C. 2004, J. Electroanal. Chem., 561, 203.
6. Dekanski, A. J., Stevanovic, R., Stevanovic, B. Z., Nikolic, V. and Jovanovic, M. 2001, Carbon, 39, 1195.
7. Chen, P. and McCreery, R. L. 1996, Anal. Chem., 68, 3958.
8. DuVall, S. and McCreery, R. L. 2000, J. Am. Chem. Soc., 122, 6759.
9. Czerwinski, A., Dmochowska, M., Grden, M., Kopczyk, M., Wojcik, G., Młynarek, G., Kołata, J. and Skowronski, J. M. 1999, J. Power Sources, 77, 28.
10. Premkumar, J. and Khoo, S. B. 2004, Electrochem. Comm., 6, 984.
11. Wang, J. and Frelha, B. A. 1982, Anal. Chem., 54, 861.
12. Vaudano, F. and Tissot, P. 2001, Electrochim. Acta, 46, 875.
13. Mattiello, L. and Rampazzo, L. 1997, Electrochim. Acta, 42, 2257.
14. Szanto, D., Trinidad, P. and Walsh, F. C. 1998, J. Appl. Electrochem., 28, 251.
15. Sullivan, M. G., Kotz, R. and Haas, O. 2000, J. Electrochem. Soc., 147, 308.
16. Sullivan, M. G., Schnyder, B., Bartsch, M., Alliata, D., Barbero, C., Imhof, R. and Kotz, R. 2000, J. Electrochem. Soc., 147, 2636.
17. Maltoz, M. and Newman, J. 1986, J. Elecrochem. Soc., 133, 1850.
18. Windner, R. C., Sousa, M. F. B., and Bertazzoli, R. 1998, J. Appl. Electrochem., 28, 201.
19. Cheng, T. T. and Gyenge, E. L. 2006, Electrochim. Acta, 51, 3904.
20. Jenkins, G. M. and Kawamura, K. 1976, Polymeric Carbons, Carbon Fibre, Glass and Char; University Press: Cambridge, England.
21. Hutton, H. D., Alsmeyer, D. C., McCreery, R. L., Neenan, T. X. and Callstrom, M. 1992, Polym. Mater. Sci. Eng., 67, 237.
22. McDermott, M. T., McDermott, C. A, and McCreery, R. L. 1993, Anal. Chem., 65, 937.
23. McDermott, C. A. and McCreery, R. L. 1994, Langmuir, 10, 4307.
24. Howard, H. D., Pocard, N. L., Alsmeyer, D., Schueller, O. J. A., Spontak, R. J., Huston, M. E., Huang, W., McCreery, R. L., Neenan, T. and Callstrom, M. 1993, Chem. Mater., 5, 1727.

25. Hutton, H. D., Huang, W., Alsmeyer, D., Kometani, J., McCreery, R. L., Neenan, T. and Callstrom, M. R. 1993, Chem. Mater., 5, 1110.
26. Aoki, Y. 1993, PhD Thesis, University of Bath.
27. Wang, J. 1981, Electrochim. Acta, 26, 1721.
28. Liu, S., Miller, B. and Chen, A. 2005, Electrochem. Comm., 7, 1232.
29. Vaik, K., Schiffrin, D. J. and Tammeveski, K. 2004, Electrochem. Comm., 6, 1.
30. Gu, H., Xu, Y., Peng, W., Li, G., and Chen, H.-Y. 2004, Microchim. Acta., 146, 223.
31. McCreery, R. L. 1991, Carbon electrodes: Structural effects on electron transfer kinetics. Electroanalytical chemistry, V. 17. In: Bard, A. J. (Ed.) Marcel Dekker, New York, p. 221.
32. Engstrom, R. C. 1982, Anal. Chem., 54, 2310.
33. Engstrom, R. C. and Strasser, V. A. 1984, Anal. Chem., 56, 136.
34. Bowers, M. L. and Yenser, B. A. 1991, Anal. Chim. Acta, 243, 43.
35. Millan, K. M., Spurmanis, A. J. and Mikkelsen, S. R. 1992, Electroanalysis 4, 929.
36. Noel, M., Santhanam, R., Ravikumar, M. K. and Flora, M. F. 1995, Electroanalysis 7, 370.
37. Beilby, A. L., Sasaki, T. A. and Stern, H. M. 1995, Anal. Chem., 67, 976.
38. Gu, H. Y., Yu, A. M. and Chen, H. Y. 2001, Anal. Lett., 34, 2361.
39. Shiu, K. K. and Shi, K. 2000, Electroanalysis, 12, 134.
40. Saleh, M. M., Awad, M. I., Okajima, T., Suga, K. and Ohsaka T. 2007, Electrochim. Acta, 52, 3095.
41. Kiema, G. K., Aktay, M. and McDermott, M. T. 2003, J. Electroanal. Chem., 540, 7.
42. Korshin, G.V. 1998, J. Electroanal. Chem., 446, 13.
43. Kiema, G. K., Fitzpatrick, G. and Mcdermott, M. T. 1999, Anal. Chem., 71, 4306.
44. Ilangovan, G. and Pillai, K. C. 1997, J. Electroanal. Chem., 431, 11.
45. Dekanski, A., Stevanovic, J., Stevanovic, R. and Jovanovic, V. M. 2001, Carbon, 39, 1207.
46. Yang, Y. and Lin, Z. 1996, Synth. Met., 78, 111.
47. Shi, K. and Shiu, K. K. 2002, Anal. Chem., 74, 879.
48. Nagaoka, T. and Yoshino, T. 1986, Anal. Chem., 58, 1037.
49. Turyan, I. and Mandler, D. 1993, Anal. Chem., 65, 2089.
50. Wang, H.-S., Ju, H.-X. and Chen, H.-Y. 2002, Anal. Chim. Acta, 461, 243.
51. Li, N. B., Luo, H. Q. and Chen, G. N. 2004, Anal. Bioanal. Chem., 380, 908.
52. Premkumer, J. and Khoo, S. B. 2005, J. Electroanal. Chem., 576, 105.
53. Tammeveskia, K., Kontturi, K., Nichols, R. J., Potter, R. J. and Schiffrin D. J. 2001, J. Electroanal. Chem., 515, 101.
54. Maruyama, J. and Abe, I. 2001, Electrochim. Acta, 46, 3381.
55. Maruyama, J. and Abe, I. 2002, J. Electroanal. Chem., 527, 65.
56. Alkire, R. and Gracon, B. 1975, J. Electrochem. Soc., 122, 1594.
57. Saleh, M. M., Awad, M. I., Kitamura, F. and Ohsaka, T. 2006, Electrochim. Acta, 51, 6331.
58. Beck, N., Meech, S., Norman, P. and Pears, L. 2002, Carbon, 40, 531.
59. Wang, Z., Kanoh, H., Kaneko, K., Lu, G. and Do, D. 2002, Carbon, 40, 1231.
60. Lee, W. and Lee, J. 2001, Appl. Surf. Sci., 171, 136.
61. Moulder, J. F., Stickle, W. F., Sobol, P. E. and Bomben, K. D. 1992, in: J. Chastain (Ed.), Handbook of X-ray Photoelectron Spectroscopy, Perkin-Elmer, Eden Prairie: MN, p. 25.
62. Yumitori, S. 2000, J. Mater. Sci., 35, 139.
63. Beccat, P., Da Silva, P., Huibon, Y. and Kasztelan, S. 1999, Oil Gas Sci. Tech., 54, 487.
64. Nagoaka, T., Sakai, T., Ogura, K. and Yoshino, T. 1986, Anal. Chem., 58, 1953.
65. Saleh, M. M., El-Ankily, M. H., El-Deab, M. S. and El-Anadouli, B. E. 2006, Bull. Chem. Soc. Jpn., 79, 1711.
66. El-Deab, M. S. and Saleh, M. M. 2003, Int. J. Hydrogen Energy, 28, 1199.
67. Bohme, O., Leidich, F. U., Salge, H. J. and Wendt, H. 1994, Int. J. Hyd. Energy, 19, 349.

68. Rausch, S. and Wendt, H. 1996, J. Electrochem. Soc., 143, 2852.
69. Brown, I. J. and Sotiropoulos, S. 2000, J. Appl. Electrochem., 30, 107.
70. Saleh, M. M. 2004, J. Phys. Chem. B, 80, 13419.
71. Nagoaka, T. and Yoshino, T. 1986, Anal. Chem., 58, 1037.
72. Guppta, N. and Oloman, C. W. 2006, J. Appl. Electrochem., 36, 255.
73. Da Pozzo, A., Di Palma, L., Merli, C. and Petrucci, E. 2005, J. Appl. Electrochem., 35, 413.
74. Drogui, P., Elmaleh, S., Rumeau, M., Bernard, C. and Rambaud, A. 2001, J. Appl. Electrochem., 31, 877.
75. Gyenge, E. L. and Oloman, C. 2005, J. Elecrochem. Soc., 152, D42.
76. Strong, W. R., Knauff, A. R., Fravel, B. W. and Samide, M. J. Carbon 44 (2006) 1936.
75. Do, J.-S. and Chen, C. P. 1994, J. Appl. Electrochem., 24, 936.
76. Qiang, Z., Chang, J-H. and Huang, C-P. 2002, Water Res., 36, 85.
77. Gallegos, A. A. and Pletcher, D. 1998, Electrochim. Acta, 44, 853.
78. Kim, H. and Popov, B. N. 2003, J. Electrochem. Soc., 150, D56.
79. Toupin, M., Brousse, T. and Belanger, D. 2004, Chem. Mater., 16, 3184.
80. Lee, H. Y., Manivannan, V. and Goodenough, J. B. 1999, Comptes Rendus Chimie, 2, 565.
81. Djurfors, B., Broughton, J. N., Brett, M. J. and Ivey, D. G. 2003, J. Mater. Sci., 38, 4817.
82. Jeong, Y. U. and Manthiram, A. 2002, J. Electrochem. Soc., 149, A1419.
83. Reddy, R. N. and Reddy, R. G. 2003, J. Power Sources, 124, 330.
84. Subramanian, V., Zhu, H., Vajtai, R., Ajayan, P. M. and Wei, B. 2005, J. Phys. Chem. B, 109, 20207.
85. Izumiya, K., Akiyama, E., Habazaki, H., Kumagai, N., Kawashima, A. and Hashimoto, K. 1998, Electrochim. Acta, 43, 3303.
86. Abdel Ghany, N. A., Kumagai, N., Meguro, S., Asami, K. and Hashomoto, K. 2002, Electrochim. Acta, 48, 21.
87. El-Deab, M. S. and Ohsaka T. 2008, J. Electrochem. Soc., 155, D14.
88. El-Deab, M. S. and Ohsaka T. 2006, J. Electrochem. Soc., 153, A1365.
89. El-Deab, M. S. and Ohsaka T. 2007, Electrochim.Acta, 52, 2166.
90. El-Deab, M. S., Awad, M. I., Mohammad, A. M. and Ohsaka T. 2007, Electrochem. Commun., 9, 2082.
91. Mohammad, A. M., Awad, M. I., El-Deab, M. S., Okajima, T. and Ohsaka, T. 2008, Electrochim. Acta, 53, 4351.
92. El-Deab, M. S. and Ohsaka T. 2006, Angew. Chem. Int. Ed., 45, 5963.
93. Kiros, Y. and Schwartz, S. 1991, J. Power Sources, 36, 547.
94. Kaimakis, T. 1993, J. Power Sources 45, 219.
95. Cao, Y. L., Yang, H. X., Al, X. P. and Xiao, L. F. 2003, J. Electroanal. Chem., 557, 127.
96. Vogel, W. and Lundquist, J. T. 1970, J. Electrochem. Soc., 117, 886.
97. Kiros, Y., Lindstron, O. and Yang, J., XU, J. J. 2003, Electrochem. Commun., 5, 306.
98. Beni, G., Schiavone, L. M., Shay, J. L., Dautremont-Smith, W. C. and Schneider, B. S. 1979, Nature, 282, 281.
99. El-Deab, M. S., El-Shakre, M. E., El-Anadouli, B. E. and Ateya, B. G. 1996, Int. J. Hydrog. Ener., 21, 273.
100. El-Deab, M. S., El-Shakre, M. E., El-Anadouli, B. E. and Ateya, B. G. 1996, J. Appl. Electrochem., 26, 1133.
101. Suredini, H. B., Cerne, J. L., Crnkovic, F. C., Machado, S. A. S. and Avaca, L. A. 2000, Int. J. Hydrog. Ener., 25, 415.
102. Prosini, P. P., Pozio, A., Botti, S. and Ciardi, R. 2003, J. Power Sources, 118, 265.
103. Wei, Z. D., Ji, M. B., Chen, S. G., Liu, Y., Sun, C. X., Yin, G. Z., Shen, P. K. and Chan, S. H. 2007, Electrochim. Acta, 52, 3323.
104. Bocca, C., Barbucci, A. and Cerisola. G. 1998, Int. J. Hydrogen Energy, 23, 247.
105. Kibria, M. F. and Mridha, M. 1996. Int. J. Hydrogen Energy, 21, 179.
106. Carapuc, H. M., Pereira, M. I. S. and da Costa, F. M. A. 1990, Mat. Res. Bull., 25, 1183.

107. Kibria, A. K. and Tarafdar, S. A. 2002, Int. J. Hydrogen Energy, 27, 879.
108. Schannon, R. D. 1976, Acta Cryst., A32, 751.
109. Iwakura, C., Honji, A. and Tamura, H. 1981, Electrochim. Acta, 26, 1319.
110. Trasatti, S. 1994, Lipkowski, J, Ross, P. N., editors. Electrochemistry of novel materials. New York: VCH Publishers Inc., p.207.
111. Tavares, A. C., da Silva, M. I. P., Mendonc, M. H., Nunes, M. R., da Costa, F. M. A. and Sa, C. M. 1998, J. Electroanal. Chem., 449, 91.
112. Morita, M., Iwakura, C. and Tamura, H. 1978, Electrochim. Acta, 23, 331.
113. Tavares, A. C., Cartaxo, M. A. M., da Silva, M. I. P. and Costa, F. M. 1999, J. Electroanal. Chem., 464, 187.
114. Kawashima, A., Asami, K. and Hashimoto, K. 1999, Mater. Sci. Eng., A267, 254.
115. Legros, R., Metz, R. and Rousset, A. 1990, J. Mater. Sci., 25, 4410.
116. Fujimura, T., Matsui, T., Habazaki, H., Kawashima, A., Kumagai, N. and Hashimoto, K. 2000, Electrochim. Acta, 45, 2297.
117. Hiroi, M., Muroya, M., Tada, E. and Ogawa, S. 1989, Denki Kagaku, 57, 837.
118. Roche, I., Chainet, E., Chantenet, M. and Vondrak, J. 2007, J. Phys. Chem. C, 111, 1434.
119. Vondrak, J., Klapste, B., Velicka, J., Sedlarikova, M., Novak, V., Reiter, J., Roche, I., Chainet, E., Fauvarque, J. F. and Chatenet, M. 2005, J. New Mater. Electrochem. Syst., 8, 209.
120. Pourbaix, M. 1966, "Atlas of Electrochemical Equilibria in Aqueous Solutions", Pergamon Press, London.
121. Lima, F. H. B., Calegaro, M. L. and Ticianelli, E. A. 2006, Russ. J. Electrochem., 42, 1283.
122. Fundo, A. M. and Abrantes, L. M. 2006, Russ. J. Electrochem., 42, 1291.
123. Deabate, S. and Henn, F. 2005, Electrochim. Acta, 50, 2823.
124. Jozwiak, W. K., Mitros, M., Kałuzna-Czaplińska, J. and Tosik, R. 2007, Dyes Pigm., 74, 9.
125. Serdar, O., Bulent, Z. and Kiroglu, F. 2006, J. Food Eng., 75, 396.
126. Von Gunten, U. 2003, Wat. Res., 37, 1469.
127. Leshem, E. N., Pines, D. S., Ergas, E. G. and Reckhow, D. A. 2006, J. Environm. Eng., 132, 324.
128. Zhao, W., Wu, Z. and Wang, D. 2006, J. Hazard Mater. B, 137, 1859.
129. Yasuda, M. 2005, Electrochem. Solid State Lett., 8, J13.
130. Oztekin, S., Zorlugenc, B. and Zorlugenc, F. K. 2006, J. Food Eng., 75, 396.
131. Foller, P. C. and Kelsall, G. H. 1993, J. Appl. Electrochem., 23, 996.
132. Silva, L. M. D., Franco, D. V., Forti, J. C., Jardim, W. F. and Boodts, J. F. C. 2006, J. Appl. Electrochem., 36, 523.
133. Amadelli, R., Armelao, L., Velichenko, A., Nikolenko, N. V., Girenko, D. V., Kovalyov, S. V. and Danilov, F. I. 1999, Electrochim. Acta, 45, 713.
134. Silva, L. M. D., De Faria, L. A. and Boodts, J. F. C. 2003, Electrochim. Acta, 48, 699.
135. Amadelli, R., Armelao, L., Velichenko, A. B., Nikolenko, N. V., Girenko, D. V., Kovalyov, S. V. and Danilov, F. I. 1999, Electrochim. Acta, 45, 713.
136. Chernik, A. A., Drozdovich, V. B. and Zharskii, I. M. 1997, Russ. J. Electrochem., 33, 259.
137. Stucki, S., Baumann, H., Christen, H. J. and Kotz R. 1987, J. Appl. Electrochem., 17, 773.
138. Babak, A. A., Amadelli, R., De Battisti, A. and Fateev, V. N. 1994, Electrochim. Acta, 39, 1597.
139. Stucki, S., Theis, G., Kotz, R., Devantay, H. and Christen, H. 1985, J. Electrochem. Soc., 132, 367.
140. Amadelli, R., De Battisti, A., Girenko, D. V., Kovalyov, S. V. and Velichenko, A. B. 2000, Electrochim. Acta, 46, 341.
141. Ota, K., Kaida, H. and Kamiya, N. 1987, Denki Kagaku Oyobi Kogyo Butsuri Kagaku 55, 465.
142. Shepelin, V. A., Babak, A. A., Potatova, G. F., Kasatkin, E. V. and Roginskaya, Y. E. 1990, Elektrokhimiya, 26, 1142.
143. Foller, P. C. and Goodwin, M. L. 1984, Ozone Sci. Eng., 6, 29.

144. Foller, P. C. and Tobias, W. 1982, J. Electrochem. Soc., 129, 506.
145. Rice, R. G. 1982, A. Netzer (Eds.), Handbook of Ozone Technology and Applications, vol. 1, Ann Arbor Science, UK.
146. Feng, J., Johnson, D. C., Lowery, S. N. and Carey, J. J. 1994, J. Electrochem. Soc., 141, 2708.
147. Tatapudi, P. and Pallav, J. M. 1993, J. Electrochem. Soc., 140, 3527.
148. Wen, T. C. and Chang, C. C. 1993, J. Electrochem. Soc., 140, 2764.
149. Wen, T. C. and Chang, C. C. 1992, J. Chin. Inst. Chem. Eng., 23, 397.
150. Chernik, A. A., Drozdovich, V. B. and Zharskii, I. M. 1997, Russ. J. Electrochem., 33, 264.
151. Zhou, Y., Wu, B., Gao, R., Zhang, H. and Jiang, W. 1996, Yingyong Huaxue, 13, 95.
152. Fateev, V. N., Akelkina, S. V., Velichenko, A. B. and Girenko, D. V. 1998, Russ. J. Electrochem., 34, 815.
153. Babak, A. A., Amadelli, R. and Fateev, V. N. 1998, Russ. J. Electrochem., 34, 149.
154. Velichenko, A. B., Girenko, D. V., Kovalyov, S. V., Gnatenko, A. N., Amadelli, R. and Danilov, F. I. 1998, J. Electroanal. Chem., 454, 203.
155. Amadelli, R., Armelao, L., Velichenko, A. B., Nikolenko, N. V., Girenko, D. V., Kovalyov, S. V. and Danilov, F. I. 1999, Electrochim. Acta, 45, 713.
156. Da Silva, L. M., De Faria, L. A. and Boodts, J. F. C. 2001, Pure Appl. Chem., 73, 1871.
157. Katsuki, N., Takahashi, E., Toyoda, M., Kurosu, T., Lida, M., Wakita, S., Nishiki Y. and Shimamune, T. 1998, J. Electrochem. Soc., 145, 2358.
158. Foller, P. C. and Tobias, W. 1981, J. Phys. Chem., 85, 3231.
159. Kotz, E. R. and Stucki, S. 1987, J. Electroanal. Chem., 228, 407.
160. Da Silva, L. M., De Faria, L. A. and Boodts, J. F. C. 2003, Electrochim. Acta, 48, 699.
161. Suzuki, H., Murashima, T., Shimizu, K. and Tsukamoto, K. 1991, Chem. Lett., 20, 817.
162. Otwell, W. S., Blake, N., Sweat, D. E., Rice, R. G., Marschalk, R. and Farquhar, J. 1985, Proc. 7th Ozone World Congr., p. 271.
163. Black, A. P. and Christman, R. F. 1963, J. Am. Water Works Assoc., 55, 897.
164. Pichet, P. and Hurtubise, C. 1975, Proc. 2nd Int. Sym. Ozone, p. 664.
165. Abe, N., Fujino, K. and Ban, Y. 1987, J. Electrochem. Soc., 134, 2041.
166. Taube, H. 1959, Trans. Faraday Soc., 53, 656.
167. Nakayama, S., Esaki, K., Namba, K., Taniguchi, Y. and Tabata, N. 1979, Ozone Sci. Eng., 1, 119.
168. Beck, T. R. and Moulton, R. W. 1956, J. Electrochem. Soc., 103, 247.
169. Chernik, A. A., Drozdovich, V. B. and Zharskii, I. M. 1997, Elektrokhimiya, 33, 289.
170. Tatapudi, P. and Fenton, J. M. 1994, J. Electrochem. Soc., 141, 1174.
171. Yeo, I. H., Kim, S., Jacobson, R. and Johnson, D. C. 1989, J. Electrochem. Soc., 136, 1395.
172. de Vitt, J. E. and Johnson, D. C. 1990, J. Electrochem. Soc., 137, 3071.
173. Babak, A. A., Fateev, V. N., Amadelli, R. and Potapova, G. F. 1994, Elektrokhimiya, 30, 814.
174. Foller, P. C. and Tobias, C. W. 1981, J. Phys. Chem., 85, 3238.
175. La Course, W. R., Hsiao, J. L. and Johnson, D. C. 1989, J. Electrochem. Soc., 136, 3714.
176. de Mussy, J-P. G., Macpherson, J. V. and Delplancke, J-L. 2003, Electrochim. Acta, 48, 1131.
177. Tseung, A. C. C., Yeh, S., Liu, X., Kelsall, G. H. and Dykstra, P. 1990, Novel Acid Resistant Oxygen Evolution Electrodes, Commission of the European Communities, p. 19, London, UK.
178. Foller, P. C. and Kelsall, G. H. 1993, J. Appl. Electrochem., 23, 996.
179. Awad, M. I., Saleh, M. M. and Ohsaka, T. 2006, J. Electrochem. Soc., 153, D207.

180. Czerwinski, A. 1995, Pol. J. Chem., 69, 699.
181. Gyenge, E. L. and Oloman, C. W. 2003, J. Appl. Electrochem., 33, 665.
182. Hozle, R. and Castro, A. M. L. 1988, J. Appl. Electrochem., 18, 679.
183. Gallegos, A. A. and Pletcher, D. 1999, Electrochim. Acta, 44, 2483.
184. Dobos, D. 1975, Electrochemical Data, p. 512, Elsevier, New York.
185. Kraft, A., Stadelmann, M., Wunsche, M. and Blaschke, M. 2006, Electrochem. Commun., 8, 883.
186. Saleh, M. M., Weidner, J. W. and Ateya, B. G., 1995, J. Electrochem. Soc., 142, 4113.
187. Saleh, M. M., Awad, M. I. and Ohsaka, T. 2008, J. Solid-State Electrochem., 12, 251.
188. Graves, J. E., Pletcher, D., Clarke, R. L. and Walsh, F. C. 1992, J. Appl. Electrchem., 22, 200.
189. Semchenko, P., Lyubushkina, E. T. and Lyubushkin, V. 1973, Electrokhimiya, 9, 1744.
190. Seader, J. D. and Tobias, C. W. 1952, Ind. Eng. Chem., 44, 2207.
191. Santana, M. H. P., De Faria, L. A. and Boodts, J. F. C. 2004, Electrochim. Acta, 49, 1935.
192. Wang, Y. H., Cheng, S., Chan, K. and Li, X. Y. 2005, J. Electrochem. Soc., 152, D197.